Reduced Electrical Bandwidth Receivers for Direct Detection 4-ary PPM Optical Communication Intersatellite Links

Final Report on NASA Grant NAG5-1510

Frederic M. Davidson
Xiaoli Sun

Department of Electrical and Computer Engineering
The Johns Hopkins University
Baltimore, Maryland 21218-2868

ABSTRACT

The receiver frontend design is studied in detail for free-space direct detection optical communication systems that uses an avalanche photodiode photodetector and 4-ary pulse position modulation (PPM) signal format. The optimal receiver contains a filter which should act as a weighted integrator. The bandwidth of the optimal filter, which should be infinite in theory, in practice must be at least several times the reciprocal of the optical PPM pulse width. A suboptimal receiver design which contains a raised cosine filter was analyzed and tested. The major advantage of the raised cosine filter receiver is that the electrical bandwidth required is always less than the reciprocal of the PPM pulsewidth. The difference in receiver sensitivity between the optimal receiver and the raised cosine receiver is shown to be less than 1.0 dB.

February 1993

1. Introduction

One of the major source of noise in a direct detection optical communication receiver is the shot noise due to the quantum nature of the photodetector. The shot noise is signal dependent and is neither Gaussian nor wide sense stationary. When a photomultiplier tube (PMT) or an avalanche photodiode (APD) is used, there is also an multiplicative excess noise due to the randomness of the internal photodetector gain. Generally speaking, the radio frequency (RF) communication theory cannot be applied to direct detection optical communication systems because noise in RF communication systems is usually additive and Gaussian. In this report, we first derive a receiver structure which is mathematically optimal for signal dependent shot noise. Several suboptimal receiver structures are discussed and compared with the optimal receiver. The objective is to find a receiver structure which is easy to implement and gives close to optimal performance.

In direct detection optical communication systems which use Q-ary PPM signaling formats, L binary source bits, which occur at the rate of one every T_B seconds, are transmitted over the channel as a single light pulse confined to one of $Q=2^L$ times slots, each of duration $\tau=LT_B/Q$ seconds. Figure 1 shows an example for a 4-ary PPM signal format. The optimal detection scheme which minimizes the receiver bit error rate (BER) is maximum likelihood (ML) detection [1]. A true ML receiver must compute the values of the likelihood function for each of the Q possible PPM symbols and then compare them to find the largest one. The likelihood functions are the probability density functions of the received signal given that the k^{th} PPM symbol is sent, where $k=0,1,...,Q-1$. The likelihood functions, or their equivalents, may be generated by sampling the output of a properly designed filter which we call a ML filter. Figure 2 shows a block diagram of a maximum likelihood 4-ary PPM receiver.

The ML filter for a RF communication receiver under additive white Gaussian noise (AWGN) can be shown to consists of matched filter whose impulse response is

the same or proportional to the input signal pulse shape reversed in time. ML filters in direct detection optical communication systems are often too complicated to build in practice, with the exception of a few simple input pulse shapes. A ML filter for Q-ary PPM signal format requires infinite bandwidth since its impulse response has to be confined to within a PPM slot time to avoid intersymbol interference (ISI). In practice, an approximate ML filter or a suboptimal filter has to be used. There is always a trade-off between receiver performance, electrical bandwidth requirements, hardware complexity, and cost.

It has been shown [2] that the receiver bandwidth required for zero intersymbol interference can be as small as one half the PPM slot rate. The input laser pulses are assumed to be bandwidth limited and to have finite rise and fall times. The receiver must contain a special filter to properly reshape the pulses output from the photodetector. The filters of interest for direct detection optical communication receivers are the so called raised cosine filters whose output in response to an input pulse is a raised cosine pulse. Although raised cosine filter are not ML filters, the penalty in receiver sensitivity, which amounts to about 0.5dB, is considered well justified for the multi-fold reduction in receiver frontend electrical bandwidth. The exact raised cosine filter derived from the theory cannot be implemented since it is not a causal linear system. We will discuss several approximate but otherwise implementable forms of raised cosine filters.

Two approximate raised cosine filters, one Bessel lowpass filter and one RC filter, were tested with a 50 Mbps and 220 Mbps 4-ary PPM receivers. Measurement results of the receiver performance were close to the theoretical predictions.

2. Maximum Likelihood Receiver

We first derive the ML receiver for an ideal photodetector which has infinite bandwidth and the only source of noise is the shot noise due to the quantum nature of photon absorptions. The output of the photodetector can be modeled as a series of discrete photon counts which follow a Poisson distribution [3] with intensity function (count rate) given by

$$\lambda(t)=\eta P_o(t)/hf \tag{1}$$

where η is the quantum efficiency of the photodetector, hf the photon energy, and $P_o(t)$ the optical power incident on the photodetector active area. The number of detected photons, n, in any given interval is a Poisson random variable and the probability density function for the photon absorption times $t_1, t_2, \ldots, t_n$, is given by [3]

$$p(t_1, t_2, \ldots, t_n \,|\lambda(t)) = \{\prod_{i=1}^{n} \lambda(t_i)\} \exp[-\int_{t_0}^{t_0+T} \lambda(t)dt] \tag{2}$$

where t_0 and T are the start and the duration of the counting interval, respectively.

The photon count rate can be written as the sum of two components, one due to the received optical signal, $\lambda_s(t)$, and the other due to background radiation, λ_0, as

$$\lambda(t)=\lambda_s(t)+\lambda_0 \tag{3}$$

where the background and signal light are assumed statistically independent. For Q-ary PPM signaling,

$$\lambda_s(t) = \lambda_s^{(k)}(t) = \lambda_s p(t-k\tau), \tag{4}$$

$$k=0,1,2,\ldots,Q-1, \quad \frac{1}{\tau}\int_{-\infty}^{\infty} p(t)dt=1$$

where $p(t)$ is the normalized pulse shape function, τ is the PPM slot time, and k indicates the time slot containing the PPM light pulse. The maximum likelihood receiver determines the value of k such that Equation (2) is maximum for the set of

the observed photon absorption times, t_i, i=1,2,...,n. The log likelihood function, after discarding irrelevant terms, becomes [4]

$$l\,(k\,|t_1,\ldots,t_n) = \sum_{i=1}^{n} ln\,[1+\frac{\lambda_s^{(k)}(t_i)}{\lambda_0}]$$

$$= \int_0^{Q\tau} \{ln\,[1+\frac{\lambda_s^{(k)}(t)}{\lambda_0}]\}[\sum_{i=1}^{n}\delta(t-t_i)\,]\,dt \qquad (5)$$

The right hand side of (5) may be interperted as the output of a linear maximum likelihood filter sampled at $t=Q\tau$. The input to the filter consists of the sum of Dirac delta function impulses, each occurring at one of the photon absorption times. The ML filter impulse response is given by

$$h_{ML}^{(k)}(t)=ln\,[1+\frac{\lambda_s^{(k)}(Q\tau-t)}{\lambda_0}] = \ln[1+\frac{\lambda_s}{\lambda_0}p(t-k\tau)] \qquad (6)$$

It should be noted that the ML filter for a direct detection optical communication receiver is not a matched filter in the sense that $h_{ML}(t)$ has the same shape as $p(t)$, except for the case of rectangular input light pulses, for which $p(t-k\tau)=constant$, $(k-1)\tau\leq t\leq k\tau$. The duration of the impulse response given in (6) is the same as that of the input laser pulse and is therefore finite. Theoretically, the frequency response of the exact ML filter must extend to infinity. Consequently, the receiver frontend electrical bandwidth, up to the ML filter, must also be infinite, at least in theory.

In practice, thermal noise due to signal conditioning amplifiers, which follow the photodetector, is also present. A PMT or an APD is often used to internally multiply the primary photocurrent to overcome this circuit thermal noise. However, photodetectors with gain, especially APDs, also introduce so-called excess noise caused by the randomness of the primary photo current multiplication gain mechanism. As a result, the exact likelihood function which includes the effects of thermal and excess noises becomes very complicated and so is the exact ML filter. Nevertheless, the filter given by (6) may still be used as an approximation and we still call it a ML

filter.

The ML filter given in (6) may be implemented approximately as a tapped delay line filter, which is also called a transversal filter [5], as shown in Figure 3. We assume the taps are evenly spaced within the pulse width of the impulse response of the ideal filter. If the filter impulse response, $h(t)$, is a real and even function, the weighting factors are given by

$$a_{m_t} = h\left(m_t \Delta\tau - \frac{M-1}{2}\tau \right), \quad m_t = 0,1,...,M-1 \tag{7}$$

where $\Delta\tau$ is the delay time between taps and M is the total number of taps. The Fourier transform of the transversal filter output can be written as

$$H_{tf}(\omega) = \sum_{m_t=0}^{M-1} a_{m_t} e^{-j\omega m_t \Delta\tau} . \tag{8}$$

The spectrum given by (8) is a periodic function with period $1/\Delta\tau$ Hz. Therefore, a lowpass filter is required after the transversal filter to block out the duplicate spectrums at nonzero center frequencies. The cutoff frequency of the lowpass filter should include the main lobe and a few side lobes of the spectrum but should not exceed $1/2\Delta\tau$ Hz. The larger the number of taps, the closer the spectrum (8) approaches that of the ideal ML filter.

For the ML filter given by (6) and an orthogonal PPM signal set, we choose $\Delta\tau = \tau/M$. The weighting factors can be found by substituting (6) into (7) for $k=0$. The resultant filter is in fact a weighted integrator with photons detected at the rising and falling edges weighted more heavily than photons at the peak of received light pulses. Since the weights are dependent on the signal to noise ratio of the received optical signal, λ_s/λ_0, the ML filter has to have an additional subsystem which independently estimates the received signal and noise levels.

For rectangular PPM pulse shapes, the filter given by (6) becomes an integrator and the ML receiver must simply count the number of photoelectrons recorded over

each PPM time slot and then compare them to find the largest one. The weighting factors of the transversal filter are all equal and can be taken as unity. The spectrum of an ideal integrator is a sinc function which contains an infinite number of side lobes. A reasonably good integrator should contain at least the main and the first side lobes of the spectrum. This would contain 95% of the energy of the filter impulse response. Therefore, a reasonably good transversal filter should have at least four taps and the lowpass filter cutoff frequency should be $B_{LPF}= 2/\tau$ Hz. Such a transversal filter has been successfully implemented in a 50 Mbps 4-ary PPM direct detection optical communication system [6]. The electrical bandwidth of the receiver frontend up to the ML filter has to be greater than or equal to $M/2\tau$ Hz, $M\geq 4$. For a binary or quaternary PPM signal format, the photodetector and the subsequent linear amplifier have to have electrical bandwidths which are at least two times the reciprocal of the pulse width, or four times the source binary data rate. A complete performance analysis, namely, the receiver bit error rate (BER) versus received optical signal power, of this type of PPM receiver is given in [7].

We have assumed, in this section, an orthogonal PPM signal set, that is, the input laser pulse shape is strictly confined within a PPM slot time. If the input pulse shape spills over to the adjacent time slots due to finite rise and fall times, the outputs from the ML filter cannot return to zero at the end of the next PPM time slot, causing potentially severe intersymbol interference. The receiver frontend electrical bandwidth and the laser pulse shape requirements are the major obstacles to be overcome in implementing true ML filters in high data rate direct detection PPM optical communication systems.

3. Reduced Bandwidth Raised Cosine Filter Receiver.

It has long been known in RF communication theory that signal can be transmitted over a band limited channel without intersymbol interference by proper design of the pulse shape [2]. The pulse shapes that are widely used are such that the output of the filter at receiver has the temporal and spectrum forms given by

$$y(t) = \frac{sin(\pi t/\tau)}{\pi t/\tau} \cdot \frac{cos(\beta \pi t/\tau)}{1-(2\beta t/\tau)^2}, \quad 0 \leq \beta \leq 1 \tag{9}$$

$$Y(\omega) = \tau \times \begin{cases} 1, & |f\tau| \leq \frac{1-\beta}{2} \\ \frac{1}{2}[\,1-sin(\frac{|\omega|\tau-\pi}{2\beta})\,], & 1-\beta < |\frac{\omega\tau}{\pi}| < 1+\beta \\ 0, & otherwise. \end{cases} \tag{10}$$

where β is called the roll-off factor. Figure 4 shows plots of (9) and (10) for several value of β. We call the filter at the receiver which produces the pulse shape given by (9) the raised cosine filter.

A raised cosine filter is in fact an equalizer. The system function of the raised cosine filter is obtained by dividing (10) by the Fourier transform of the input pulse shape. The spectrum of a raised cosine filter is confined between one half to one times the reciprocal of the average input pulse width, depending on the value of β. The bandwidth of the receiver frontend is no more than half that required by a transversal ML filter. There is no intersymbol interference in spite of the ringing in the output of the filter because the ringing crosses zero at multiples of τ, as shown in Figure 4.

In RF communication systems, it is possible to design the signal pulse shape such that the Fourier transforms of the input pulse shape and the impulse response of the matched filter are both equal to the square root of (10). The RF receiver can then achieve ML detection with finite bandwidth but no intersymbol interference. Unfortunately, a ML filter in an direct detection optical PPM communication system

is not a conventional matched filter but is given by (6). There is no known solution for an input laser pulse shape, $p(t)$, which satisfies (6) and (9) simultaneously.

Raised cosine filters are nevertheless attractive for use in direct detection optical PPM communication systems to accomplish a trade-off between receiver performance and electrical bandwidth requirements. In what follows, we assume the laser PPM pulse shapes are trapezoidal, or equivalently, rectangular with equal and finite rise and fall times. We further assume that the average pulsewidth is equal to the PPM slot time because this is often the case in practice. Such trapezoidal input pulses extend outside a PPM slot time and ML filters can no longer be used without introducing serious intersymbol interference. One of the major advantages of a raised cosine filter receiver is that it does not restrict the input pulses shapes to be within a PPM slot time and yet still gives minimum intersymbol interference. The Fourier transform of a trapezoidal pulse is given by

$$P(\omega) = sinc(\frac{\omega\tau}{2})\ sinc(\frac{\omega t_r}{2}) \tag{11}$$

where t_r is the full pulse rise time (from 0 to 100%) of the trapezoidal pulse shape. The transfer function of a raised cosine filter with β=1 under this condition is given by

$$H(\omega) = \frac{\tau(1+\cos\frac{\omega\tau}{2})}{sinc(\frac{\omega\tau_{av}}{2})sinc(\frac{\omega t_r}{2})}, \quad |\omega| < 2\pi/\tau\ . \tag{12}$$

Figure 5 shows a plot of (12) and its inverse Fourier transform with t_r=0.2τ. The transfer functions and their inverse Fourier transforms of raised cosine filters with β= 0.5 and 0.1 are also plotted in Figure 5. The shape of the curves varies only slightly for other values of t_r from 0 to 0.3τ. The inverse Fourier transforms in Figure 5 were obtained numerically. Since (12) is a real and even function, the inverse Fourier transform of (12), which is the filter impulse response, is also real. The filter may be

implemented as a transversal filter with real weights in each delay arm.

4. Receiver Performance When Using Raised Cosine Filters

The receiver BER of a Q-ary PPM receiver is related to the PPM word error rate (WER) by [8]

$$BER = \frac{Q}{2(Q-1)} WER \tag{13}$$

The PPM word error rate can be computed as

$$WER = 1 - \int_{-\infty}^{\infty} p(x\,|1)\,[\int_{-\infty}^{x} p(x'\,|0)dx']^{Q-1}\,dx$$

$$\approx (Q-1)\int_{-\infty}^{\infty} p(x\,|1)\int_{x}^{\infty} p(x'\,|0)dx'\,dx \tag{14}$$

where $p(x\,|1)$ and $p(x'\,|0)$ are the probability density functions of the signal output from the raised cosine filter sampled at the ends of the time slots with and without a PPM pulse present, respectively. The exact forms of the probability density functions are too complicated to derive and it is a common practice to approximate the filter output as Gaussian random variables with the same means and variances. The Gaussian approximation has been shown to give satisfactory results when compared with experimental measurements except when the effective background noise level is below a few detected noise photoelectrons per PPM slot time or the average APD gain is relatively low [7]. Using the Gaussian approximation and substituting (14) into (13),

$$BER = \frac{Q}{4}\frac{1}{\sqrt{2\pi}\sigma_1}\int_{-\infty}^{\infty} e^{-\frac{(x-\bar{x}_1)^2}{2\sigma^2}}\, erfc(\frac{x-\bar{x}_0}{\sqrt{2}\,\sigma_0})\,dx. \tag{15}$$

where $\bar{x}_1$, $\bar{x}_0$, σ_1^2, and σ_0^2 are the means and variances of the filter output when a

PPM pulse is present and absent, respectively, and $erfc(x)$ is the standard complimentary error function.

APD photodetectors are used in most of direct detection optical communication systems that contain AlGaAs semiconductor laser diode transmitters ($\lambda \sim 800$nm). The mean and variance of the signal output from the raised cosine filter due to the APD photocurrent alone are given by [3]

$$E\{y_o(t)\} = qG \int_{-\infty}^{\infty} \lambda(\sigma) h(t-\sigma) d\sigma + (GI_b + I_s) \int_{-\infty}^{\infty} h(\sigma) d\sigma \tag{16}$$

$$var\{y_o(t)\} = q^2 G^2 F \int_{-\infty}^{\infty} \lambda(\sigma) h^2(t-\sigma) d\sigma + (qG^2 F I_b + qI_s) \int_{-\infty}^{\infty} h^2(\sigma) d\sigma \tag{17}$$

where q is the electron charge, G is the average APD gain, $h(t)$ is the impulse response of the raised cosine filter, I_b and I_s are the APD bulk and surface leakage currents, and F is the APD excess noise factor given by

$$F = k_{eff} G + (2 - 1/G)(1 - k_{eff}) \tag{18}$$

with k_{eff} the ratio of the APD ionization coefficients of holes and electrons. The detected photon count rate, $\lambda(t)$, can be written according to (3) and (4) as

$$\lambda(t) = \lambda_0 + \lambda_s \sum_{m=-\infty}^{\infty} p(t - k_m \tau - mQ\tau) \tag{19}$$

The background and signal photon count rate, λ_0 and λ_s, in (19) can be written as

$$\lambda_0 = \frac{\bar{n}_0}{\tau} = \frac{\bar{n}_{bg}}{\tau} + \frac{1}{\alpha_e} \frac{\eta P_{spk}}{hf} \tag{20}$$

$$\lambda_s = \frac{\bar{n}_s}{\tau} = (1 - \frac{1}{\alpha_e}) \frac{\eta P_{spk}}{hf} \frac{\tau_{av}}{\tau} \tag{21}$$

where $\bar{n}_0$ and $\bar{n}_s$ are the average numbers of effective detected background and signal photons per PPM slot time, $\bar{n}_{bg}$ is the actual number of detected background radiation photons per PPM slot time, P_{spk} is the received peak optical signal power,

τ_{av} is the average pulse width of the trapezoidal pulse shape, and α_e is the laser ON-OFF extinction ratio defined as the ratio of the peak to minimum optical signal power. Substituting (20) and (21) into (19) and then into (16) and (17), and rewriting the right hand sides of (16) and (17) in frequency domain, the mean and variance of the filter output, conditioned on the entire PPM word sequence, $\{k_m\}$, become

$$E\{y_o(t)\,|\{k_m s\}\} = qG\bar{n}_s \frac{1}{2\pi\tau}\int_{-\infty}^{\infty}[\sum_{m=-\infty}^{\infty} P(\omega)e^{-j\omega mQ\tau - j\omega k_m\tau}]H(\omega)e^{j\omega t}d\omega$$

$$+ [qG\bar{n}_{bg} + GI_b\tau + I_s\tau]H(0) \tag{22}$$

$$Var\{y_o(t)\,|\{k_m s\}\} =$$

$$q^2G^2F\bar{n}_s \frac{1}{2\pi\tau}\int_{-\infty}^{\infty}[\sum_{m=-\infty}^{\infty} P(\omega)e^{-j\omega mQ\tau - j\omega k_m\tau}]H(\omega)*H(\omega)e^{j\omega t}d\omega$$

$$+ [q^2G^2F(\bar{n}_{bg}+\frac{I_b\tau}{q})+\frac{I_s\tau}{q}]\frac{1}{2\pi}\int_{-\infty}^{\infty}|H(\omega)\,|^2 d\omega \tag{23}$$

where

$$H(\omega)*H(\omega) = \frac{1}{2\pi}\int_{-\infty}^{\infty} H(\omega')H(\omega-\omega')d\omega'. \tag{24}$$

For convenience, we normalize the signal such that

$$x(t) = \frac{y_{out}(t)\tau}{qR} \tag{25}$$

with R the APD load resistance. The system function of the raised cosine filter satisfies

$$P(\omega)\frac{H(\omega)}{R} = Y(\omega) \tag{26}$$

where $Y(\omega)$ is given by (10). The means of the filter output with and without a PPM pulse present can be obtained by substituting $t=k_0\tau$ and $t\neq k_0\tau$ into (22), as

$$\bar{x}_1 = E\{x(t=k_0\tau)\} = G(\bar{n}_s + \bar{n}_{bg}) + G\frac{I_b\tau}{q} + \frac{I_s\tau}{q} \tag{27}$$

$$\bar{x}_0 = E\{x(t\neq k_0\tau)\} = G\bar{n}_{bg} + G\frac{I_b\tau}{q} + \frac{I_s\tau}{q}. \tag{28}$$

The variance of the filter output sampled at the end of the time slot which contains the PPM pulse can be computed by substituting (25) and (26) into (23), letting $t=c_0\tau$, and averaging over all possible PPM patterns, $\{k_m\}$, as

$$Var\{x(t=k_0\tau)\} = G^2F\bar{n}_s\frac{\tau}{2\pi}\int_{-\infty}^{\infty}P(\omega)[\frac{Y(\omega)}{P(\omega)}*\frac{Y(\omega)}{P(\omega)}]d\omega$$

$$+G^2F\bar{n}_s\frac{\tau}{2\pi}\int_{-\infty}^{\infty}P(\omega)[\sum_{m=-\infty,\,m\neq 0}^{\infty}e^{-j\omega mQ\tau}E\{e^{j\omega(c_0-c_m)\tau}\}]\,[\frac{Y(\omega)}{P(\omega)}*\frac{Y(\omega)}{P(\omega)}]d\omega$$

$$+[G^2F(\bar{n}_{bg}+\frac{I_b\tau}{q})+\frac{I_s\tau}{q}]\,\frac{\tau}{2\pi}\int_{-\infty}^{\infty}|\frac{Y(\omega)}{P(\omega)}|^2d\omega. \tag{29}$$

If the PPM words appear equally likely, i.e., $Pr(k_m) = 1/Q$,

$$E\{e^{j\omega(k_0-k_m)\tau}\} = |E\{e^{j\omega k_m\tau}\}|^2 = \frac{\sin^2(Q\omega\tau/2)}{Q^2\sin^2(\omega\tau/2)}. \tag{30}$$

The sum of the exponentials in (29) can be rewritten as

$$\sum_{m=-\infty,\,m\neq 0}^{\infty}e^{-j\omega mQ\tau} = [\sum_{m=-\infty}^{\infty}e^{-j\omega mQ\tau}] - 1 = \frac{2\pi}{Q\tau}[\sum_{k=-\infty}^{\infty}\delta(\omega-\frac{2\pi k}{Q\tau})] - 1. \tag{31}$$

Substituting (30) and (31) into (29) and following the procedure given by Smith and Personick [9], we have

$$Var\{x(t=c_0\tau)\} = G^2F\bar{n}_sI_1 + G^2F\bar{n}_s(\Sigma_1-I_{11}) + [G^2F(\bar{n}_{bg}+\frac{I_b\tau}{q})+\frac{I_s\tau}{q}]I_2 \tag{32}$$

where

$$I_1 = \frac{\tau}{2\pi}\int_{-\infty}^{\infty} P(\omega)[\frac{Y(\omega)}{P(\omega)} * \frac{Y(\omega)}{P(\omega)}]d\omega \tag{33}$$

$$\Sigma_1 = \frac{1}{Q}\sum_{m=-\infty}^{\infty} P(2\pi m/\tau)[\frac{Y(2\pi m/\tau)}{P(2\pi m/\tau)} * \frac{Y(2\pi m/\tau)}{P(2\pi m/\tau)}] \tag{34}$$

$$I_{11} = \frac{\tau}{2\pi}\int_{-\infty}^{\infty} P(\omega)\frac{\sin^2(Q\omega\tau/2)}{Q^2\sin^2(\omega\tau/2)}[\frac{Y(\omega)}{P(\omega)} * \frac{Y(\omega)}{P(\omega)}]d\omega \tag{35}$$

$$I_2 = \frac{\tau}{2\pi}\int_{-\infty}^{\infty} |\frac{Y(\omega)}{P(\omega)}|^2 d\omega\,. \tag{36}$$

The shot noise level corresponding to the time slot which does not contain a PPM pulse depends on the distance from the slot which does contain the PPM pulse. The worst case condition occurs when the output signal is sampled at the end of the time slot which is adjacent to the time slot that contains the PPM light pulse. The variance of the shot noise under this condition can be obtained similarly to (32) and is given by

$$Var\{x(t=(c_0\pm 1)\tau\} = G^2F\bar{n}_sI_{10}$$
$$+ G^2F\bar{n}_s(\Sigma_1 - I_{11}) + [G^2F(\bar{n}_{bg}+\frac{I_b\tau}{q})+\frac{I_s\tau}{q}]I_2 \tag{37}$$

where

$$I_{10} = \frac{\tau}{2\pi}\int_{-\infty}^{\infty} P(\omega)[\frac{Y(\omega)}{P(\omega)} * \frac{Y(\omega)}{P(\omega)}]e^{j\omega\tau}d\omega. \tag{38}$$

The integrals and the summation (33), (34), (35), (36), and (38) are dimensionless and only depend on the Fourier transform of the input pulse shape function. They can be evaluated numerically once the input pulse shape is given. An example is shown in Table 1, assuming a trapezoidal input pulse shape with average pulse width equal to the PPM slot time ($\tau_{av}=\tau$).

In practice, all the amplifiers add noise to the output signal. The dominant noise source is from the photodetector preamplifier. This noise can be modeled as a zero mean Gaussian random process and appears additive to the output signal. In practice, transimpedance amplifiers with a FET frontend are often used as the preamplifier because of its stability and wide dynamic range. Figure 6 shows a typical circuit of an APD and transimpedance preamplifier. The feedback resistance, R_f, effectively serves as the APD load resistance. The variance of the total output noise due to a transimpedance preamplifier can be written similarly to [9] as,

$$Var\{v_{out}\}_{amp} = [\frac{2KT}{R_i} + \frac{2KT}{R_f} + qI_g]\frac{1}{2\pi}\int_{-\infty}^{\infty} |H(\omega)|^2 d\omega$$

$$+ \frac{1}{2\pi}\int_{-\infty}^{\infty} \frac{2KT\Gamma}{g_m} |H(\omega)|^2 \left|\frac{Z_i(\omega)+Z_f(\omega)}{Z_i(\omega)Z_f(\omega)}\right|^2 d\omega \qquad (39)$$

where K is Boltzmann's constant, T is the temperature ($^\circ$K), R_i and R_f are the input and feedback resistances, I_g is the FET gate leakage current, $2KT\Gamma/g_m$ is the spectral density of the series input voltage noise of the amplifier, Γ is a parameter close to unity, g_m is the FET transconductance, $Z_i(\omega)$ and $Z_f(\omega)$ are the total input and feedback impedances. For a good transimpedance amplifier, $R_i >> R_f$, $C_i >> C_f$, and (39) can be approximated as

$$Var\{V_{out}\}_{amp} \approx (\frac{2KT_e}{R_f} + qI_g)\frac{1}{2\pi}\int_{-\infty}^{\infty} |H(\omega)|^2 d\omega$$

$$+ \frac{1}{2\pi}\frac{2KT\Gamma}{g_m}\int_{-\infty}^{\infty} \frac{1+(R_fC_i\omega)^2}{R_f^2} |H(\omega)|^2 d\omega . \qquad (40)$$

The second term in (40) corresponds to a noise whose power spectral density grows proportionally to the square of the frequency as $f >> 1/2\pi R_f C_i$. Therefore, it is important to keep the total input capacitance, which consists of the amplifier input capacitance and the photodetector shunt capacitance, as low as possible. The value of $R_f C_i$ is usually of the order 10^{-9} second in a high speed optical communication

system. Consequently, the noise spectral density is nearly flat at low frequency and starts to increase rapidly as the frequency exceeds about 100 *MHz*.

In practice, however, the feedback resistances of most of commercially available transimpedance amplifiers are relative small so that the first term of (40) dominates and the total amplifier noise power spectrum appears constant. Under this condition, an equivalent noise temperature, T_e, can be defined such that the total amplifier noise is equal to the noise generated by the feedback resistance at effective temperature T_e (°K). The total amplifier noise, which is normalized according to (25), can be written, to a good approximation, as

$$Var\{x\}_{amp}=\frac{2KT_e\tau}{q^2R_f}\cdot\frac{\tau}{2\pi}\int_{-\infty}^{\infty}\left|\frac{Y(\omega)}{P(\omega)}\right|^2 d\omega=\frac{2KT_e\tau}{q^2R_f}I_2 \tag{41}$$

where I_2 is given by (36).

The variance of the total noise at the output of the raised cosine filter is the sum of (41) and (32) or (37), so that

$$\sigma_1^2=G^2F\bar{n}_sI_{10}+[G^2F(\bar{n}_{bg}+\frac{I_b\tau}{q})+\frac{I_s\tau}{q}]I_2+\frac{2KT_e}{q^2R_f}\tau I_2 \tag{42}$$

$$\sigma_0^2=G^2F\bar{n}_sI_{10}+G^2F\bar{n}_s(\Sigma_1-I_{11})+[G^2F(\bar{n}_{bg}+\frac{I_b\tau}{q})+\frac{I_s\tau}{q}]I_2+\frac{2KT_e}{q^2R_f}\tau I_2 \tag{43}$$

where the values of I_1, Σ_1, I_{11}, I_2, and I_{01} are given by (33)—(36), and (38).

When the input pulse shape is perfectly rectangular and an optimal receiver, which contains an integrator, is used, the means of the normalized filter output are still given by (42) and (43) and the variances reduce to [7]

$$\sigma_1^2=G^2F\bar{n}_s+[G^2F(\bar{n}_{bg}+\frac{I_b\tau}{q})+\frac{I_s\tau}{q}]+\frac{2KT_e}{q^2R_f}\tau \tag{44}$$

$$\sigma_0^2=[G^2F(\bar{n}_{bg}+\frac{I_s\tau}{q})+\frac{I_s\tau}{q}]+\frac{2KT_e}{q^2R_f}\tau. \tag{45}$$

The receiver BER can be computed by substituting (27), (28), (42), and (43) into (15). The analysis presented in this section also applies for arbitrary input pulse shapes and receiver filters provided the proper Fourier transforms of the input pulse shape function and the filter impulse response are used when evaluating the integrals and the summation of (33)—(36) and (38).

5. Numerical Results

Calculations of receiver performance are presented in this section. The Gaussian approximation described in the previous section was used, which is most accurate when the average number of photons due to finite laser ON-OFF extinction ratio and background radiation is greater than one per PPM slot time. Since a practical optical intersatellite link is likely to be operated under very low background radiation but a finite laser ON-OFF extinction ratio, the values of n_{bg}=0 and α_{ext}=25 were used in most cases for the numerical computations. Optimal values of the average APD gain were found by exhaustive search. Other system parameters were chosen to be the typical values used in our experimental system and these are listed in Table 2. The receiver performance at different extinction ratios from 100 to 5 is shown at end of this section. The roll-off factor, β, was assumed equal to unity throughout this section.

Figure 7 shows the receiver BER as a function of received peak optical signal power in dBm. The solid curve corresponds to rectangular input pulse shape with an optimal integrator receiver and the dashed curve corresponds to the same rectangular input pulse shape and a raised cosine filter receiver. The optimal APD gain was found to be G_{opt}=200 for both cases. It is shown in Figure 7 that the penalty caused by using a raised cosine filter receiver is about 0.5dB at a $BER=10^{-6}$. This was also confirmed by a direct computer simulation using the Block-Oriented System

Simulator (BOSS) reported in [10].

Figure 8 shows the receiver BER as a function of the received peak optical signal power for rectangular, trapezoidal, and raised cosine input pulse shapes, all confined within a PPM slot time, as shown in Figure 9. The trapezoidal pulse shape was assumed to be symmetric with rise time t_r=0.2τ. As shown in Figure 8, the receiver BER increases as the input light pulse shape narrows for a fixed received peak signal power. This is because the average number of signal photons, or energy, per PPM pulse for trapezoidal and raised cosine input pulses is less than that of the rectangular input pulse of the same peak power. The average number of detected signal photons per PPM pulse is $(\overline{n}_s)_{trapzd} = (1-t_r/\tau)(1-1/\alpha_{ext})\lambda_{spk}\tau$ for trapezoidal input pulses and $(\overline{n}_s)_{rcos} = (1/2)(1-1/\alpha_{ext})\lambda_{spk}\tau$ for raised cosine input pulses. It is clear that the optimal input pulse shape under both peak and average power limits is a rectangular pulse of width τ. The trapezoidal and raised cosine input pulses require higher received peak power than that of rectangular input pulses in order to achieve the same receiver BER.

Figure 10 shows an example of receiver performance of a raised cosine filter receiver (dotted curve) compared to a matched filter receiver (dashed curve) when the input pulse shape is a raised cosine function. The matched filter receiver performance is considerably worse (1.6dB in P_{spk} for $BER=10^{-6}$) because of the larger noise bandwidth required to match to the raised cosine input pulse ($f_0=2/\tau$ instead of $1/\tau$).

Figure 11 shows the receiver BER as a function of peak received power for rectangular, confined and nonconfined trapezoidal (t_r=0.2τ) input pulse shapes as shown in Figure 12 when using a raised cosine filter receiver. It is clear that the best practical input pulse shape should be a trapezoid not confined to a single PPM time slot but with the average pulse width equal to a PPM slot time. The penalty caused by using nonconfined trapezoidal input pulse shape with a relatively slow rise time (20%

of a slot time) is only about 0.1dB as compared to the same raised cosine filter receiver with a perfect rectangular input pulse shape. However, this is only true when a raised cosine filter, not a ML filter, is used in the receiver.

Figure 13 shows a plot of receiver BER as a function of received peak optical signal power for laser ON-OFF extinction ratios 100:1, 25:1, 10:1, and 5:1 using a nonconfined trapezoidal input pulse shape with t_r=0.2τ and a raised cosine filter receiver. The laser transmitter ON-OFF extinction ratio has far more influence on the receiver performance than the input pulse shape and the receiver type.

6. Implementation of Raised Cosine Filters

A raised cosine filter may be implemented approximately using standard network synthesizing technology. A roll-off parameter of β=1.0 is desired in practice since the filter frequency response is the closest to that of a simple RC lowpass filter and the ringing in the filter output is the smallest. It is very important for a raised cosine filter to maintain a linear phase response, otherwise the output waveform will be distorted [5]. Two type of filters which give linear or close to linear phase response are transversal filters and Bessel filters.

6.1. Transversal Raised Cosine Filter

A transversal type raised cosine filter is similar to that shown in Figure 3. Since the impulse response of an ideal raised cosine filter is not confined in time domain, some delay taps are required to cover the filter response outside one PPM slot time. A truncated impulse response function has to be used to determine the weights. The cutoff frequency of the lowpass filter following the transversal filter is the same as that of the raised cosine filter.

A computer program was written to simulate the filter response using the LabView software (by National Instruments Corp.) on a McIntosh IIci computer. The number of taps required to synthesize the raised cosine filter was determined by trial and error based on computer simulations. The program used for the simulation is shown in Figure 14. The time base was normalized with respect to the PPM slot time, τ. The lowpass filter which followed the summer of the tapped delay line filter was an ordinary Chebyshev lowpass filter. A RC lowpass filter was also included to simulate the transimpedance preamplifier of the photodetector. The 3dB bandwidth of the RC lowpass filter was set equal to the reciprocal of the input pulsewidth.

We started by choosing 13 evenly spaced taps covering a time span $[-2\tau, 2\tau]$ of the impulse response, $h(t)$, of the ideal raised cosine filter with trapezoidal input pulse shape as shown in the lower part of Figure 5. We then changed the value of the roll-off factor of the raised cosine pulse shape such that the $\pm$3rd and $\pm$5th taps corresponded approximately to the filter impulse response at zero crossings, and the $\pm$4th and $\pm$6th taps to the peaks of the side lobes of the filter impulse response. The weights of the 4 taps about the zero crossings were then set to zero by skipping the taps. Therefore, we actually need only 9 taps for this evenly spaced 13 tap transversal filter. The value of the roll-off parameter which satisfied the above condition was found to be $\beta \approx 0.93$. The waveform output from the filter in response to a trapezoidal input pulse was shown to follow very closely the ideal raised cosine pulse shape.

However, when the lowpass and the RC filters were included, the pulse shape output from the filter was broadened, skewed, and did not cross zero at $t=\pm\tau$. To ensure the filter output crossed zero at $t=\pm\tau$, we changed the weights of the $\pm$4th taps from -0.105 to -0.300 and -0.200, respectively. Lastly, the two outer most ($\pm$6th) taps were found to have little effect on the output pulse shape and therefore could be eliminated.

The resultant tapped delay line filter had a total of 7 taps and their weights were 1.0 at $t=0$, 0.785 at $t=\pm 0.25\tau$, 0.324 at $t=\pm 0.5\tau$, -0.200 at $t=-\tau$ and -0.300 at $t=\tau$. Figure 15 shows the simulation result. The filter output and its power spectrum were very close to a raised cosine pulse shape with $\beta=0.7—0.9$, although the original set of weights were derived using $\beta=0.93$. The power spectra in the lower part of Figure 15 were not exactly the same as those of the Fourier transforms of the corresponding waveforms in the time domain because of the windowing effect during digital signal processing. Nevertheless Figure 15 shows the resultant tapped delay line filter gave an output which was almost identical to the output of an ideal raised cosine filter. The lowpass filter was a 3rd order Chebyshev filter with a 3dB bandwidth of $1.5\tau^{-1}$ to $2\tau^{-1}$ Hz and 0.1 dB ripples in the pass band.

The tapped delay line filter derived above can be implemented using all passive components which include broadband power splitters, coax cable delays, and attenuators, as shown in Figure 16. Negative weights were realized by an inverting transformer followed by an ordinary attenuator. The waveform output from the filter can be tailored slightly by adjusting the weights until it closely fits an ideal raised cosine pulse shape.

6.2. Bessel Lowpass Filter as Raised Cosine Filter

Bessel lowpass filters are characterized by a maximum flat phase response and a magnitude response close to a raised cosine filter with unity roll-off factor [5]. One can circumvent the difficulties in the analytical derivation of the exact raised cosine filter by using a Bessel lowpass filter to a good approximation. The two parameters of the Bessel lowpass filter, namely, the order and the 3 dB cutoff frequency, can be determined by trial and error through computer simulations. Other types of well known lowpass filters, such as Butterworth and Chebyshev filters are not considered since they tend to have very nonlinear phase responses near the cutoff frequency. A

Bessel lowpass filter can be constructed with standard network synthesizing technologies once the order and the 3 dB cutoff frequency are known.

A computer program was written to determine the optimal values of the order and the 3 dB cutoff frequency of the Bessel lowpass filter. The program was written using the LabView software, which contains a library of digital filter subroutines including Bessel lowpass filters. The program can simulate the filter output for any given input pulse shape through digital signal processing. The input to the Bessel lowpass filter consists of computer generated trapezoidal pulses. A RC lowpass filter was added before the Bessel lowpass filter to simulate the APD preamplifier. A RC highpass filter was also inserted to simulate the AC couplings of between circuit components. Figure 17 shows the entire program used for the simulations. The program used the normalized time scale, i.e., assuming the input pulsewidth is one second. The results could be scaled down to the actual time scale. The number of samples per pulsewidth was set to 200. The rise and fall times of the trapezoid pulses were 20% of the pulsewidth. The preamplifier 3 dB bandwidth was equal to the reciprocal of the PPM pulsewidth.

It was found from the simulation that the filter which gives satisfactory raised cosine output pulse shape should be a seventh order Bessel lowpass filter with a 3 dB cutoff frequency equal to 1.3 times reciprocal of the PPM pulsewidth. The higher the order of the Bessel lowpass filter, the more symmetric the output pulse shape. The higher the 3 dB cutoff frequency, the narrower the output pulse shape. However, the order of the filter should be kept minimum in order to simplify the filter design.

Figure 18 shows a printout of the simulation results. The waveforms in the upper right graticule are the trapezoidal input pulse and the pulse output from the preamplifier. The waveforms in the lower graticule are the filter output and the exact raised cosine pulse shape as a reference. The pulse output from the preamplifier is distorted somewhat due to the limited bandwidth of the preamplifier.

Nevertheless, the pulse shape output from the Bessel lowpass filter had little improvement as the preamplifier bandwidth was increased. It is therefore sufficient for the preamplifier to have a frequency response close to a RC lowpass filter with the 3 dB bandwidth equal to the reciprocal of the pulsewidth. A slightly lower preamplifier bandwidth can be compensated by a higher 3 dB cutoff frequency of the Bessel lowpass filter. In practice, the 3 dB cutoff frequency of the Bessel lowpass filter should be determined after the preamplifier is chosen.

It was also found from the simulation that the lower 3 dB cutoff frequency due to the AC coupling between amplifiers should be no greater than 0.2% of the reciprocal of the input pulsewidth. A higher cutoff frequency causes the pulses to undershot on the falling edge and consequently causes intersymbol interference.

Figure 19 shows an example circuit diagram of such a Bessel lowpass filter according to [11]. The filter should be buildable with lumped components [12].

7. Experiments

Experiments were conducted using both a 50 Mbps 4-ary PPM and a 220 Mbps 4-ary PPM direct detection optical communication systems. Both a ML filter and a raised cosine filter were used in the 50 Mbps system and receiver performance was compared. The performance of the 220 Mbps system was measured only for a raised cosine filter due to the lack of a wide band (880 MHz) and high output power (+30dBm) linear amplifier.

7.1. Performance Measurement of the 50 Mbps 4-ary PPM Receiver

The receiver BER was measured as a function of input optical power expressed as the number of received signal photons incident on the photodetector. The details of the PPM encoder and receiver electronics have been published in [13]. The

receiver originally contained a tapped delay line ML filter for rectangular input PPM light pulses. The original measurement of the receiver performance was conducted using a commercial grade silicon APD (RCA30902S) and preamplifier. The receiver had achieved a BER of 10^{-6} at 65 received signal photons per bit using an AlGaAs laser diode transmitter (Mitsubishi ML5702A, λ=820nm).

7.1.1. Receiver performance with the ML filter and a high performance APD preamplifier module.

The APD preamplifier module used in this measurement was made by Dr. Tran Van Muoi of PlessCor Optronics, Inc. and the electronic details of the module are reported in [14]. It consisted of a low noise APD mounted on a ceramic subcarrier block and a hybrid circuit transimpedance amplifier all in one RF shielded package. The feedback resistance was 5 KΩ and the 3 dB bandwidth was 220 MHz. The APD ionization coefficient ratio was measured to be k_{eff}=0.008 [14]. With this APD preamplifier module, Dr. Muoi was able to achieve a receiver BER of 10^{-6} at 85 average received signal photons per bit at 325 Mbps with an on-off-keyed (OOK) signal format [15]. This preamplifier was superior to the one we originally used in our 50 Mbps 4-ary PPM receiver which had a feedback resistance of 1.03 KΩ and a 3 dB bandwidth of 440 MHz. The APDs in both module were about the same. Since the 50 Mbps 4-ary PPM receiver required a front end bandwidth of 200 MHz, the PlessCor APD preamplifier could be substituted and the receiver sensitivity was expected to improve.

Since the APD active surface was located about 1 mm in back of a small hole in the package, it was difficult to focus the optical signal beam onto the APD active surface. In other words, not all the light incident to the APD preamplifier module was captured by the APD active area, and consequently, it was impossible to actually measure the total optical power seen by the APD when using a simple focusing

lens. The method used originally by Muoi was to monitor the APD bias current while lowering the bias voltage to 10 volts [14]. This measurement method might have been inaccurate since it in fact used the APD itself as the optical power meter. An APD operated at such a low bias voltage was not fully depleted and the quantum efficiency decreased. On the other hand, the APD gain was not necessarily reduced to unity at this low bias voltage. The measurement result was also affected by the drift of the leakage current of the APD and the biasing circuit. In order to independently and accurately measure the received optical power seen by the APD, we used a short optical fiber to couple the optical signal to the APD and held the fiber tip as close to the APD active surface as possible. The optical fiber had a numerical aperture of 0.22 and a core diameter of 50μm. When the distance from the optical fiber tip to the APD surface was much less than 1mm, the APD, which had active area of 500 μm in diameter, should have captured all the light emitted from the optical fiber tip. The average received optical power could be measured directly by placing the fiber tip in front of an independently calibrated commercial optical power meter.

The laser transmitter used was an AlGaAs laser diode (Mitsubishi ML5702A) emitting at 820 nm wavelength. The temperature control unit, the bias current source, and the modulation current driver were all provided by NASA/GSFC. The laser was biased well below its threshold current for the highest ON-OFF extinction ratio. The rise and fall times were less than 1 ns.

We first checked the method which Dr. Muoi used in measuring the received optical signal power, that is, assuming the APD gain was unity and the quantum efficiency was 80% when reverse biased at 10 volts. The laser transmitter was modulated by the 50 Mbps Q=4 PPM signal. The photocurrent of the APD was measured as a function of the input optical signal power. It showed that the APD biased at 10 volts had an average gain of not unity, but 1.3 to 1.9, assuming a 80% quantum efficiency. The pulse shape was also severely distorted due to a high input

capacitance caused by partial depletion of the device. It might have been possible that the average APD gain was closer to unity for the 325 Mbps binary OOK modulation signal that Dr. Muoi used.

The equivalent input noise current spectral density of the preamplifier was determined by measuring the power spectrum of the noise output while biasing the APD well below the breakdown voltage. The contribution from the APD could be neglected since the APD gain was sufficiently low. The measured average power spectral density at the output of the preamplifier was -146.4 dBm/Hz, which corresponded to an equivalent noise current density of 2.14 $pA/\sqrt{Hz}$, or an equivalent noise temperature of 415 ° K for the 5KΩ APD load resistor.

The APD bulk leakage current was measured by increasing the APD gain until the total noise output from the amplifier rose by about 1 dB above the noise floor of the preamplifier itself. The power spectral density due to the APD bulk leakage current was about -129 dBm/Hz at an average APD gain of G=540. The corresponding APD bulk leakage current was then 2 pA. This measurement was only approximate since the actual noise power due to the bulk leakage current was too close to the preamplifier noise floor and could not be determined accurately using our spectrum analyzer.

The receiver BER of the 50 Mbps Q=4 PPM receiver was measured as a function of the received optical signal level in terms of number of received signal photons per information bit. The laser diode transmitter was the same as that used in the original measurement (Mitsubishi ML5702A), which had rise and fall times of about 1ns. Figure 20 shows the measurement results. The solid curve in Figure 20 shows the the theoretically predicted receiver performance computed using the algorithm described in [7]. The APD gain was optimized near $BER \approx 10^{-6}$, by adjusting the APD bias voltage until the receiver BER was minimized for a fixed received optical signal level. The value of the optimal APD gain was measured to be G=310. The

theoretically predicted value of the optimal APD gain was G=225 to 250 based on the APD and preamplifier parameters extracted. It was likely that the actual noise temperature of the preamplifier was slightly higher than what we estimated, which led to an underestimate of the optimal average APD gain.

Figure 20 shows that the receiver with this APD preamplifier achieved a receiver BER of 10^{-6} at 45 received signal photons per bit (0.56nW or -62.5dBm at 50 Mbps and λ=820 nm). This receiver performance was 1.6 dB better than what we measured with the original APD preamplifier. The measured data were close to those predicted by the theory.

7.1.2. Receiver performance with the ML filter, an EG&G *Slik* APD, and a wideband preamplifier.

Slik silicon APDs are state-of-the-art photodetectors recently developed by EG&G Canada [16] which feature a 'super low ionization coefficient,' $k_{eff}\approx 0.005$ as compared to $k_{eff}\approx 0.01$–0.02 for the commercial grade devices. Typical quantum efficiency at 800 nm wavelength is about η=90%. The diameter of the active area of the APD is 100 μm. A hybrid circuit module was made by EG&G Canada which consisted of a *Slik* APD with a low noise and wide band (~1.0GHz) transimpedance preamplifier (Anadigics ATA12000 [17]). The transimpedance of the preamplifier is 1.5 KΩ. The equivalent noise current density was specified as 5.0pA/$\sqrt{\text{Hz}}$ at 500 MHz and increases with frequency. The preamplifier also contains an automatic gain control (AGC) circuit although the AGC threshold current (100μA) is much larger than our normal operation signal level ($<$1.0μA). The APD high voltage bias supply consisted of a programmable DC-to-DC converter (Analog Modules 522-2). It had an internal temperature compensation circuit and the rms output ripple was less than 5 mv.

The laser transmitter used in this and subsequent measurements was a low power single mode AlGaAs laser diode (SDL5400-C). The laser mount, the temperature control unit and the bias current supply were all made by Light Control Instruments, Inc. The modulation signal was combined with bias current with the use of a bias tee. The laser was biased below the threshold current. The pulse rise and fall times in this case were limited by the pulse shape output from the 4-ary PPM encoder (2 ns rise and fall time). The fastest measured pulse rise and fall times of the laser were 300ps and 700ps, respectively, when driven by GaAs logic ICs (400ps rise and fall times).

The electrical characteristics of the APD preamplifier module were measured. The electrical bandwidth of the module was found to be 930 MHz, as measured by a spectrum analyzer while illuminating the APD with relatively strong CW light. The preamplifier noise current density was measured to be 2.4 pA/$\sqrt{\text{Hz}}$ at 200 MHz and increased to 6.3 pA/$\sqrt{\text{Hz}}$ at 800 MHz. The maximum average APD gain was found to be less than 200 and further increasing the bias voltage caused significant pulse shape distortion at the trailing edge, possibly due to after pulsing.

Figure 21 shows the measured receiver performance. The solid curve in Figure 21 is the theoretically predicted performance based on the measured system and device parameters using the nearly exact model described in [7]. The measured average APD gain which gave the minimum receiver BER near 10^{-6} was G=140. Further increasing the APD gain caused pulse shape distortion and resulted in higher receiver BER. However, the theoretically predicted optimal average APD gain was much higher, G_{opt}=450. Therefore, if the APD could have provided a gain up to 450 without pulse shape distortion, the receiver sensitivity would have increased by 3dB, that is, the receiver would have been able to achieve a $BER \leq 10^{-6}$ at only half the input optical signal power shown in Figure 21.

7.1.3. Receiver performance with a Bessel lowpass filter , an EG&G *Slik* APD, and a wideband preamplifier.

The ML filter in the 50 Mbps 4-ary PPM receiver was then replaced by a Bessel lowpass filter as an approximate raised cosine filter. Based on the computer simulation described in the previous section, the Bessel filter which best resembles an ideal raised cosine filter for this 50 Mbps 4-ary PPM receiver should have 9 poles and a 3 dB bandwidth of 120 MHz. The actual filter used was a 9 pole (4 sections) Bessel lowpass filter with 3 dB bandwidth equal to 123 MHz (by K&L Microwave Inc.)

The receiver performance was measured again with the Bessel lowpass filter and the result is shown in Figure 22 (crosses). The measurement result with the ML filter is also shown in Figure 22 (circles). The curves in Figure 22 represent the theoretical results for the ML filter receiver using the nearly exact analysis (solid line) and Gaussian approximation (dotted line), and for raised cosine filter using the Gaussian approximation (dashed line). Those curves show that the Gaussian approximation gives almost the same result as the nearly exact analysis when a ML filter is used and the average APD gain is relatively low. They also show that use of a raised cosine filter causes little penalty in receiver sensitivity if the average APD gain is relatively low. The difference in measured receiver performance between the use of the two different filters was about 0.7 dB, which was probably due to imperfections in the Bessel lowpass filter and impedance mismatch. Unlike a tapped delay line ML filter, it was impractical for a passive Bessel lowpass filter to have 50Ω input and output impedance across the entire bandwidth.

7.2. Performance Measurement of the 220 Mbps 4-ary PPM Receiver

The performance of our 220 Mbps 4-ary PPM receiver was measured with the same laser and APD preamplifier module as described in Section 7.1.2 and 7.1.3. The details of the 220 Mbps 4-ary PPM encoder and receiver electronics have been

reported in [16] and [17]. The receiver could only use a raised cosine filter due to the lack of a high power (30dBm) wide band (880 MHz) power amplifier to drive the comparator bank. The raised cosine filter in this case was a simple RC filter which was implemented by putting a shunt capacitor at the input of an amplifier. A 6 dB attenuator was used right before the amplifier to reduce the effect of impedance mismatch. The RC filter had a 3 dB bandwidth of 300 MHz and a stopband (-20dB) of 500 MHz.

Figure 23 shows the measurement result (circles) and the theoretical result (solid curve). The receiver achieved a sensitivity of 80 received photons per bit (4.2nW average optical input signal power) under $BER \leq 10^{-6}$. The optimal average APD gain was measured to be G=79, which was once again much smaller than the theoretically predicted value, G_{opt}=200. This discrepancy was believed to result mainly from intersymbol interference due to imperfections in the laser, the APD, and the amplifiers at this high frequency. The effect of intersymbol interference always increased with the average APD gain. According to the analysis, the receiver sensitivity in the absence of intersymbol interference would have been 59 received photons per bit at an average APD gain of 200. Therefore, the estimated loss due to intersymbol interference was about 1.3 dB.

References

[1] A. D. Whalen, *Detection of Signals in Noise.* New York: Academic Press, 1971, ch. 5.

[2] J. G. Proakis, *Digital Communications.* New York: McGraw-Hill, 1983, ch. 6.

[3] D. L. Snyder, *Random Point Processes.* New York: Wiley, 1975, ch. 4 and 5.

[4] R. M. Gagliardi and S. Karp, *Optical Communication*, New York: John Wiley & Sons, 1976, ch. 7.

[5] H. J. Blinchikoff and A. I. Zverev, *Filtering in the Time and Frequency Domains*, New York: John Wiley and Sons, 1976.

[6] X. Sun, F. M. Davidson, and C. Field, '50Mbps free space direct detection laser diode optical communication system with Q=4 PPM signaling,' in *Free-Space Laser Communication Technologies II*, D. Begley and B. Seery Eds, SPIE Proceedings, vol. 1218, pp. 385-395, Jan. 1990.

[7] F. M. Davidson and X. Sun, 'Gaussian approximation versus nearly exact performance analysis of optical communication systems with PPM signaling and APD receivers,' *IEEE Trans. Commun.*, Vol. 36, No. 11, pp. 1185-1192, Nov. 1988.

[8] A. J. Viterbi, *Principles of Coherent Communication*, New York: McGraw Hill, 1966, ch. 8, p. 226.

[9] R. G. Smith and S. D. Personick, 'Receiver design for optical for optical fiber communication systems,' in *Semiconductor Devices for Optical Communication*, H. Kressel, ed., New York: Springer-Verlag, 1980, ch. 4.

[10] A. J. Martino, 'Numerical simulation of a 325 Mbit/s QPPM optical communication system,' in *Free-Space Laser Communication Technologies IV*, D. Begley and B. Seery Eds, SPIE Proceedings, vol. 1635, pp. 168-173, Jan. 1992.

[11] S. Niewiadomski, *Filter Handbook — a practical design guide*, CRC Press, Inc., Boca Raton, Florida, 1989, pp. 34-38.

[12] *Microwave and RF Component Catalog*, K&L Microwave Inc., Salisbury, Maryland, 1989.

[13] X. Sun, F. Davidson, and C. Field, '50 Mbps free space direct detection laser diode optical communication system with Q=4 PPM signaling,' in *Free-Space Laser Communication Technologies II*, D. Begley and B. Seery Eds. SPIE Proceedings, vol. 12185, pp. 385-395, Jan. 1990.

[14] T. V. Muoi, 'Extremely sensitive receiver for laser communications,' final report prepared for NASA Goddard Flight Center, Greenbelt MD 20771, under contract No. NAS5-29283, PlessCor Optronics, Inc. 20200 Sunburst St., Chatsworth, CA 91311-6289.

[15] T. V. Muoi, 'Extremely sensitive direct detection receiver for laser communications,' *Conference on Lasers and Electro-Optics (CLEO'87)*, Technical Digest Series, Vol. 9, pp. 302-304, Paper THS4.

[16] X. Sun and F. M. Davidson, 'Direct detection optical intersatellite link at 220 Mbps Using AlGaAs laser diode and silicon APD with 4-ary PPM signaling,' Interim progress report on NASA grant NAG5-356 'Optical communication with semiconductor laser diode,' for the period Sept. 1989 - Feb. 1990.

[17] X. Sun and F. M. Davidson, 'Performance measurement results for a 220 Mbps QPPM optical communication receiver with an EG&G Slik APD,' Progress report on NASA grant NAG5-510 'Reduced electrical bandwidth receivers for direct detection 4-ary PPM optical communication intersatellite links,' for the period Oct. 16, 1991 to July 15, 1992.

Table 1. Numerical Values of Equation (33)—(36) and (38).

t_r/tau	I_1	Σ_{11}	I_{11}	$\Sigma_{11}-I_{11}$	I_2	I_{10}
0.00000	1.0990	0.2819	0.2800	1.91e-03	1.1277	0.01359
0.00100	1.0990	0.2819	0.2800	1.91e-03	1.1277	0.01359
0.01000	1.0991	0.2819	0.2800	1.91e-03	1.1277	0.01360
0.02000	1.0992	0.2820	0.2801	1.91e-03	1.1279	0.01363
0.05000	1.1000	0.2823	0.2803	1.94e-03	1.1291	0.01381
0.10000	1.1030	0.2834	0.2813	2.02e-03	1.1334	0.01446
0.20000	1.1152	0.2878	0.2854	2.38e-03	1.1512	0.01712
0.30000	1.1368	0.2956	0.2926	3.02e-03	1.1825	0.02181
0.40000	1.1699	0.3076	0.3036	4.00e-03	1.2305	0.02899
0.50000	1.2182	0.3252	0.3197	5.46e-03	1.3008	0.03945

Table 2. Parameter Values Used in the Numerical Computations

PPM alphabet size	Q=4
laser wavelength	λ=820 nm
laser pulse width	τ=2 ns (250 Mbps)
APD quantum efficiency	η=77%
APD ionization ratio	k_{eff}=0.010
APD surface leakage current	I_s=12 nA
APD bulk leakage current	I_b=0.2 pA
APD load resistance	R=1000 Ω
equivalent noise temperature	T_e=1000 $^\circ$K

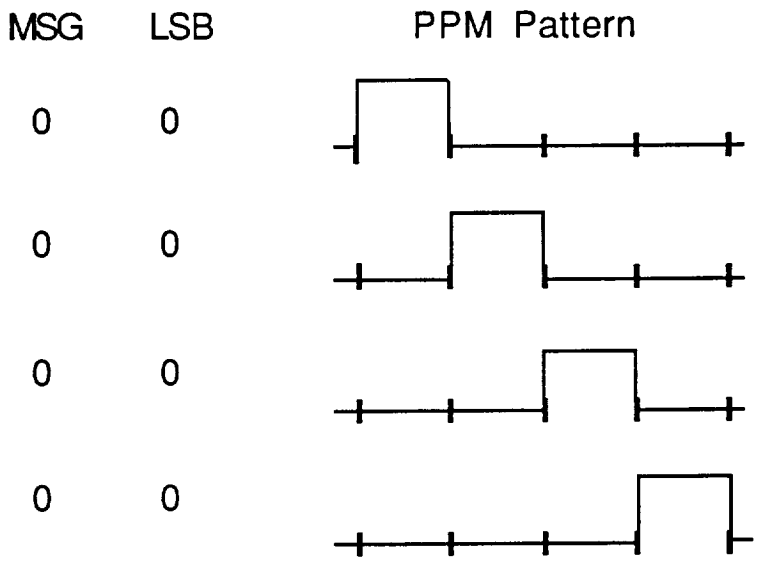

Figure 1. 4-ary PPM signaling.

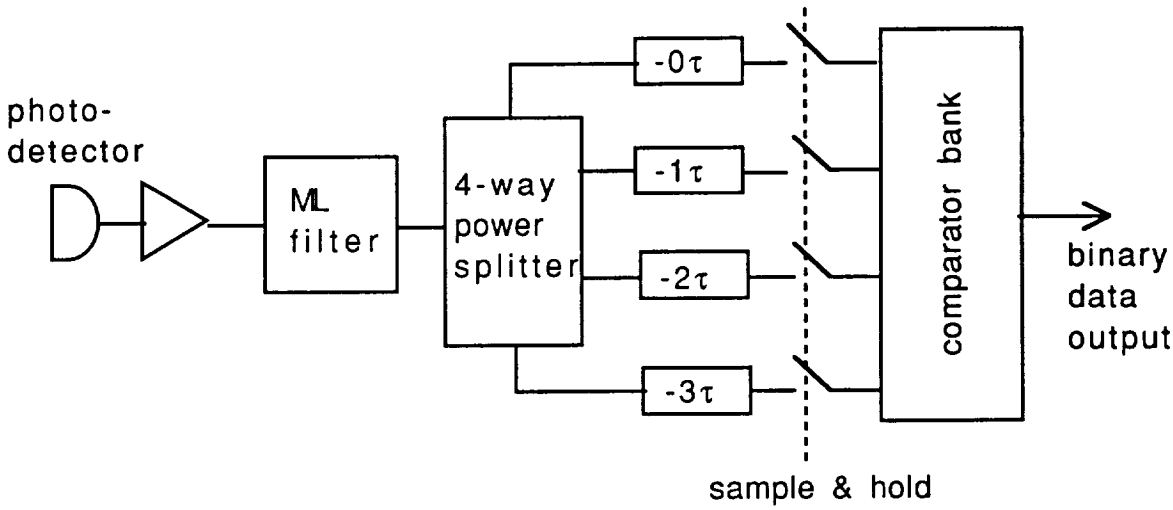

Figure 2. ML 4-ary PPM receiver.

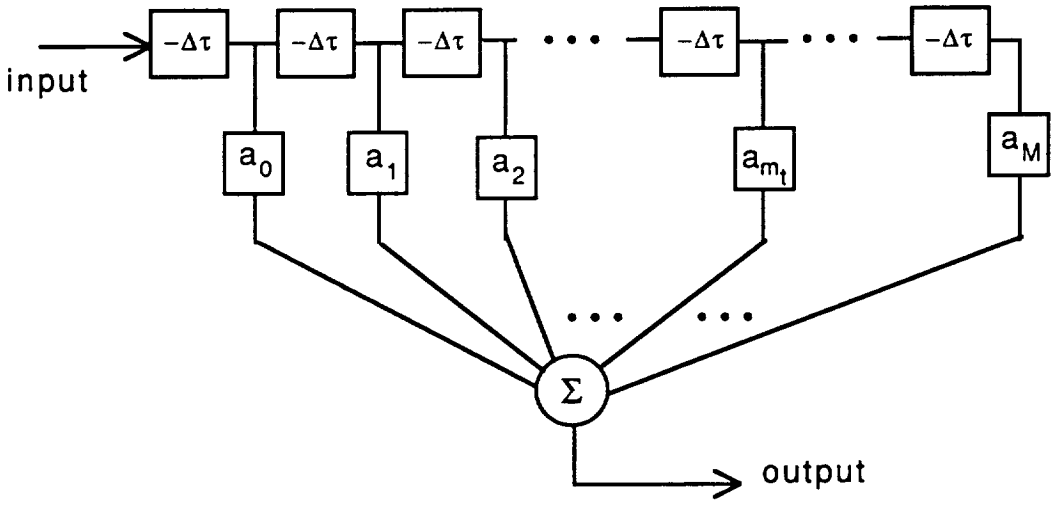

Figure 3. Block diagram of a transversal filter.

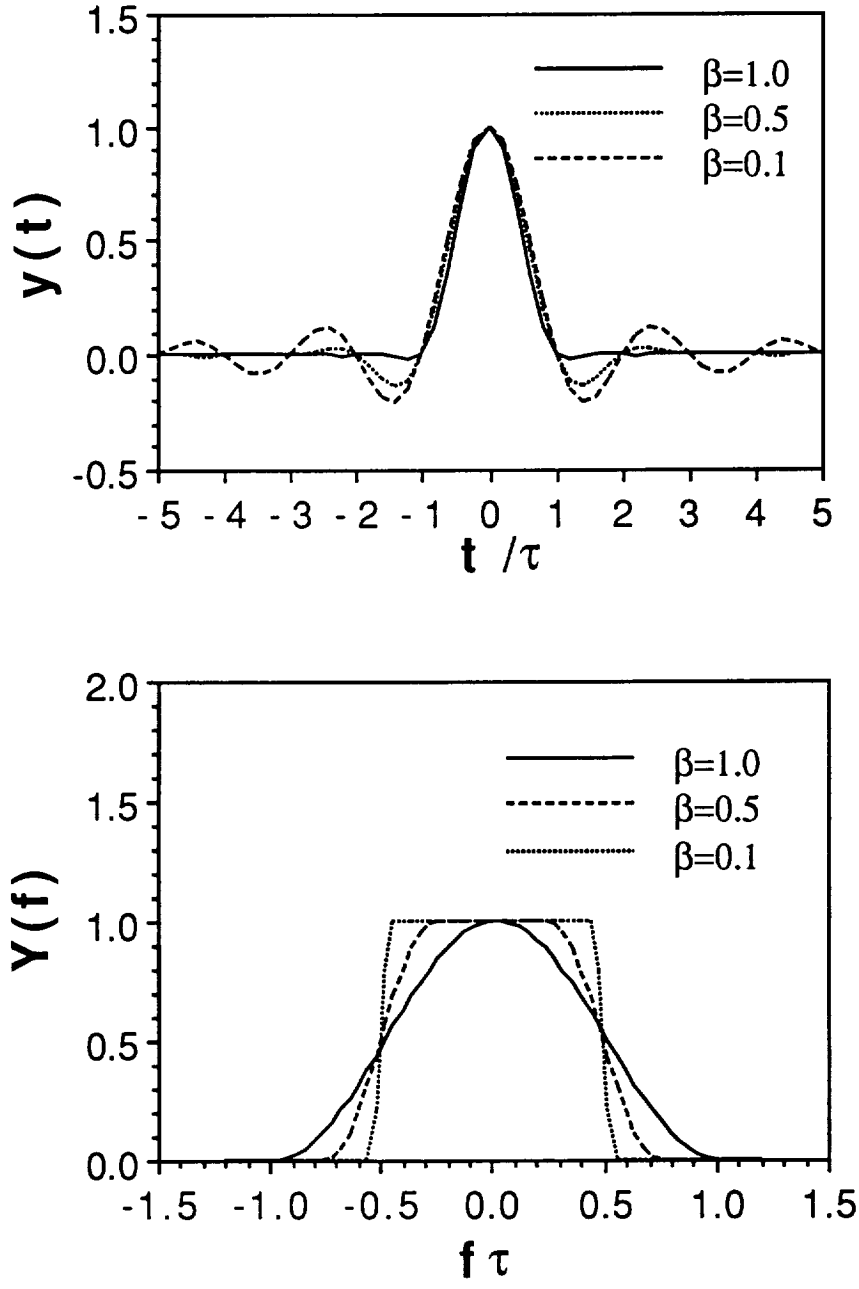

Figure 4. Raised cosine pulse shapes and their Fourier transforms for β=0.1, 0.5, and 1.0.

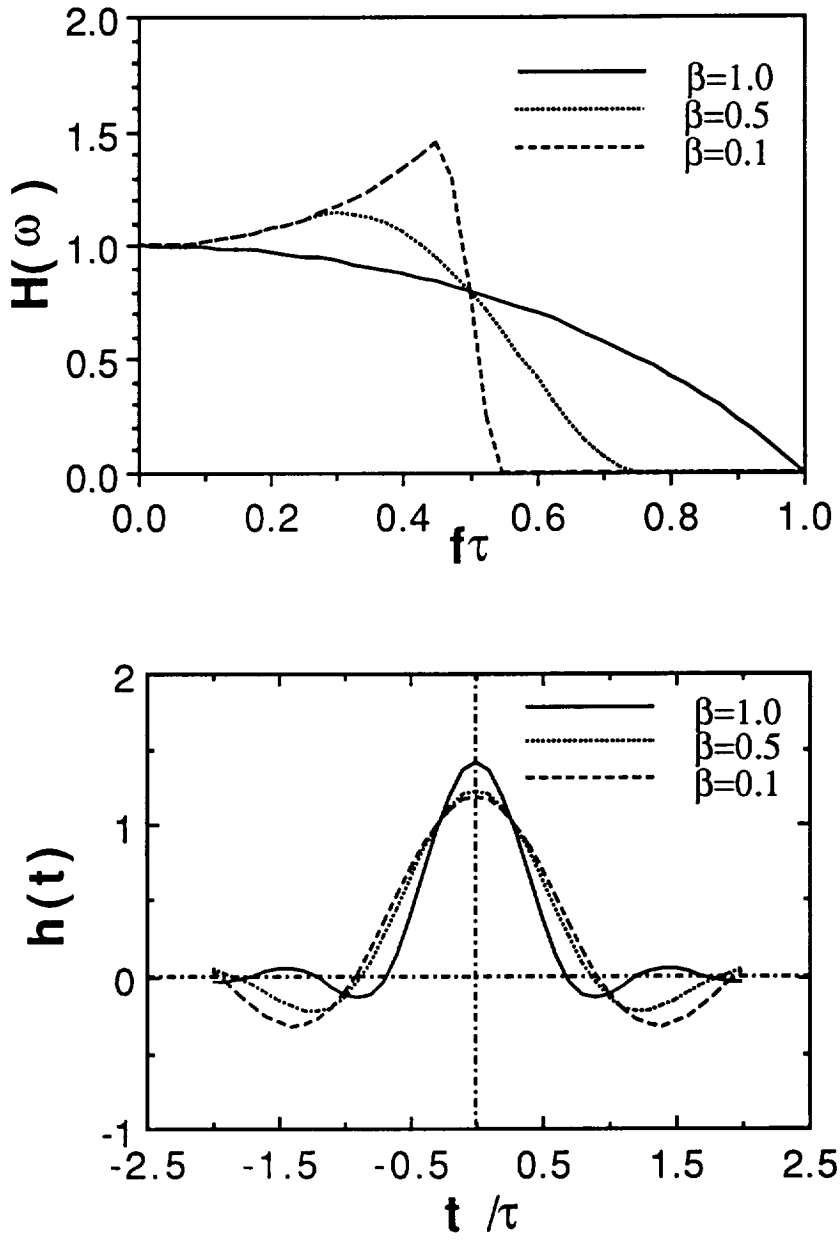

Figure 5. Raised cosine filter transfer functions and the impulse responses for trapezoidal input pulse shape with $t_r=0.2\tau$ and roll factors β =0.1, 0.5, and 1.0.

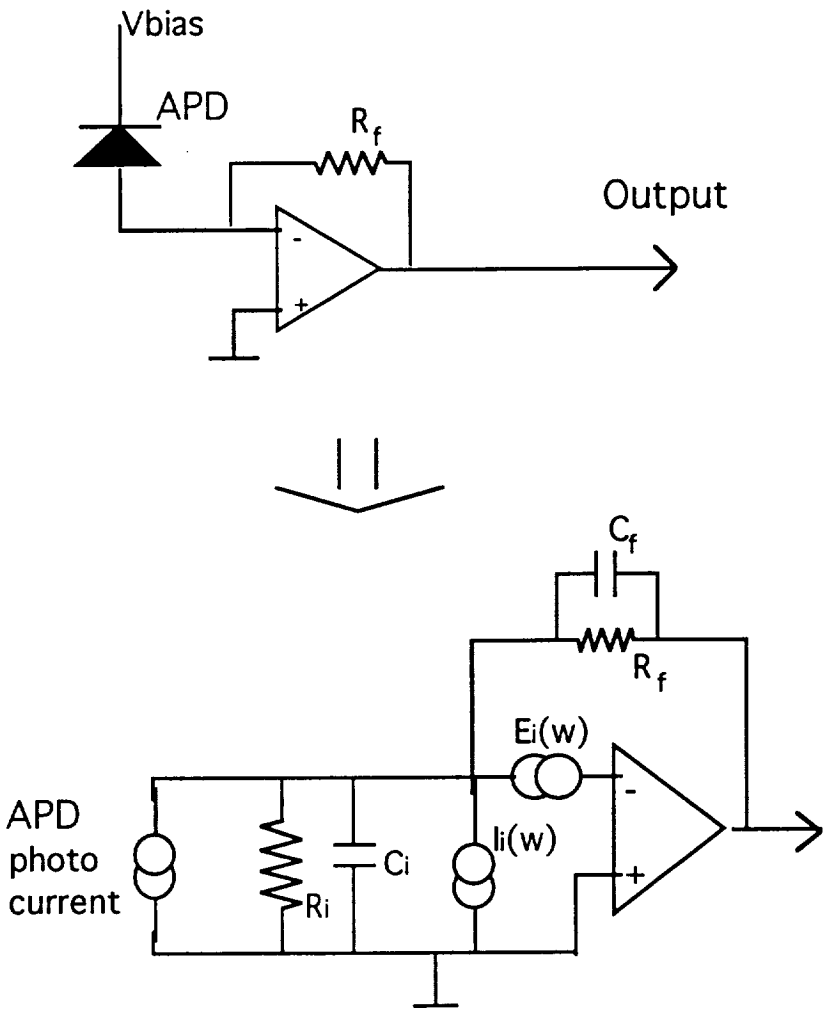

Figure 6. Transimpedance APD preamplifier circuit.

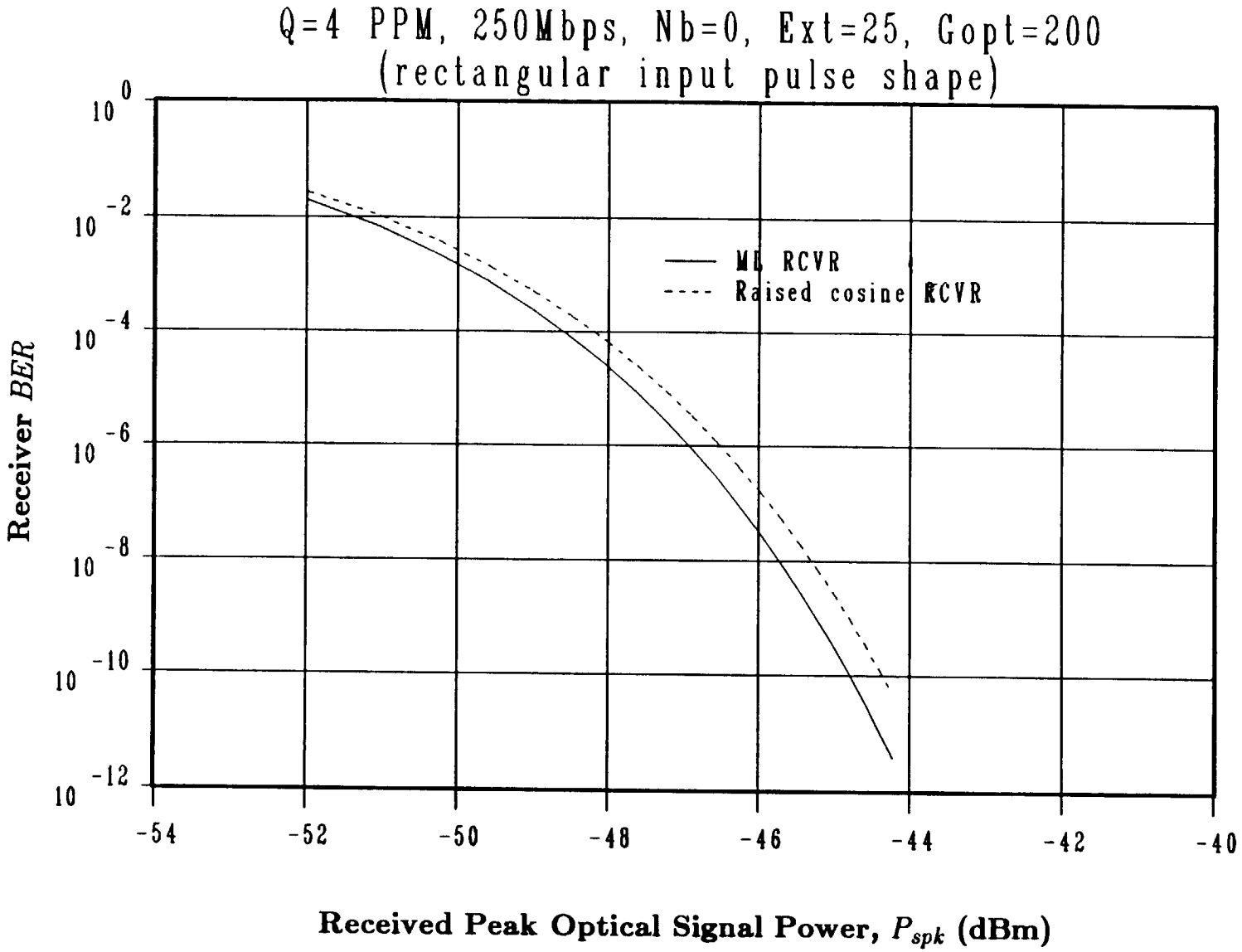

Figure 7. Receiver Performance of an ML filter receiver and a raised cosine filter receiver with rectangular input pulse shape.

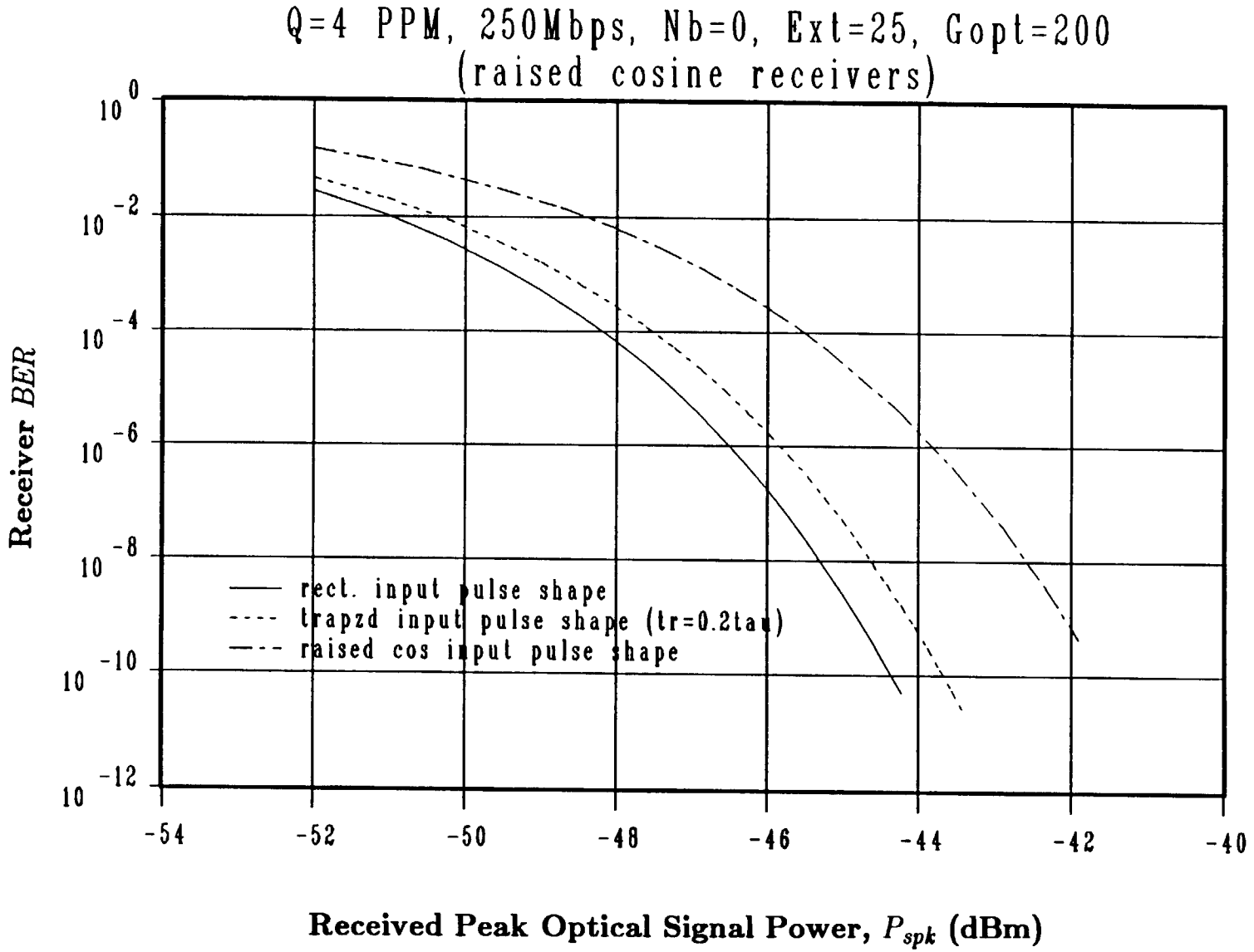

Figure 8. Performance of a raised cosine receiver with rectangular, trapezoidal, and raised cosine input pulse shapes.

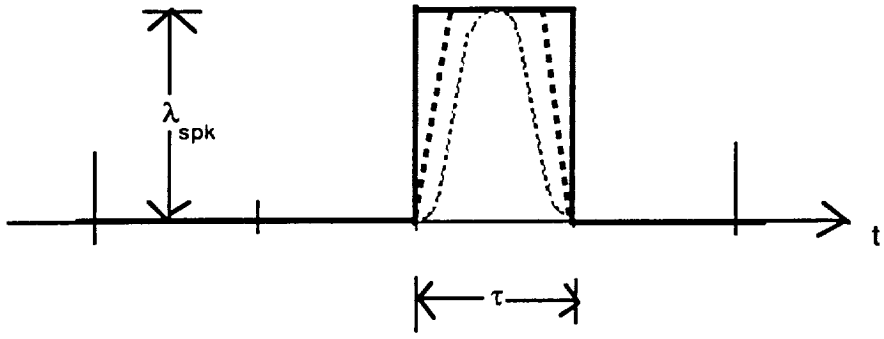

Figure 9. Rectangular (solid line), trapezoidal (heavy dashed line) and raised cosine (dotted line) input pulse shapes used for computing the curves in Figure 8.

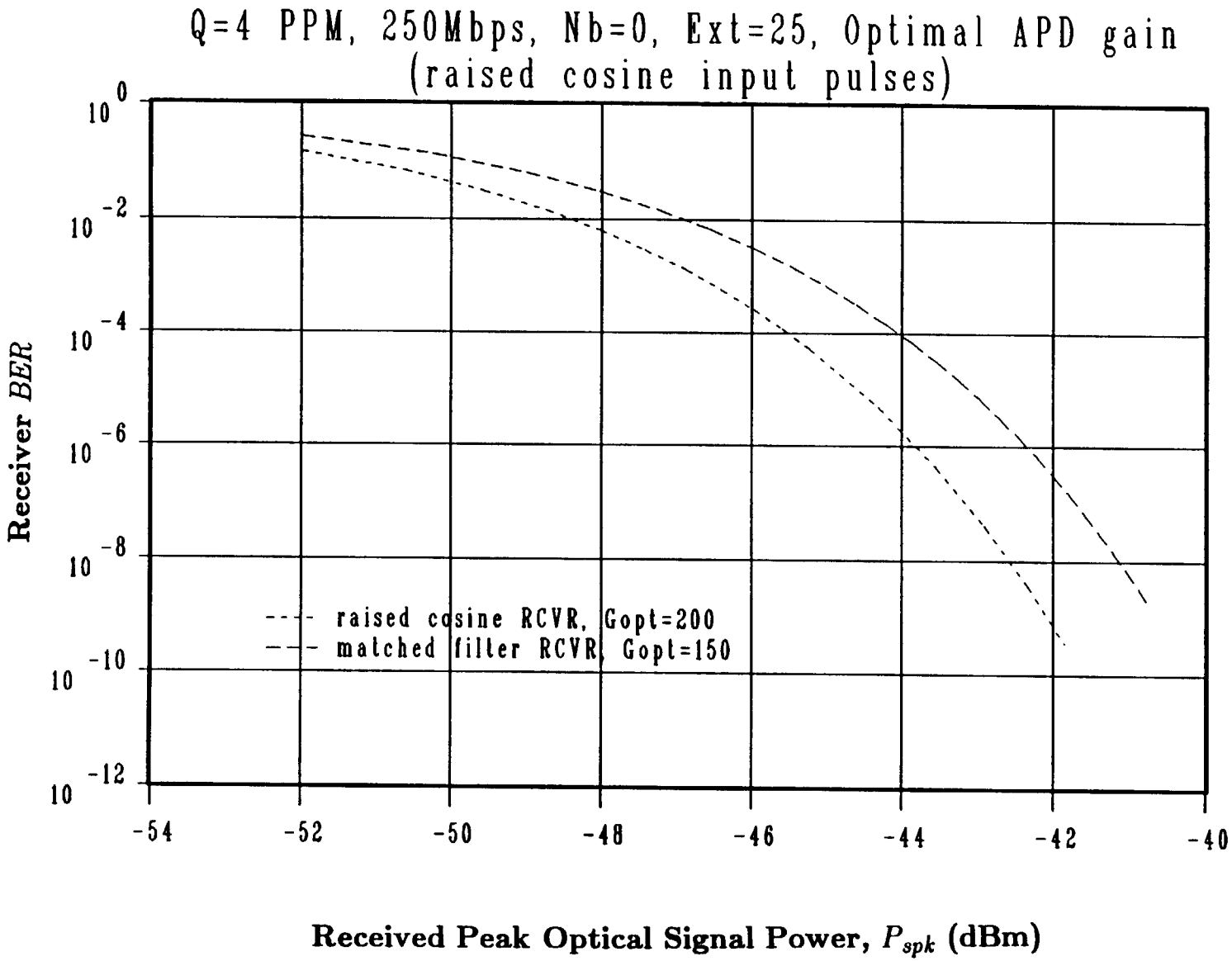

Figure 10. Performance comparison of raised cosine filter receiver and matched filter receiver for the raised cosine input pulse shape shown in Figure 9.

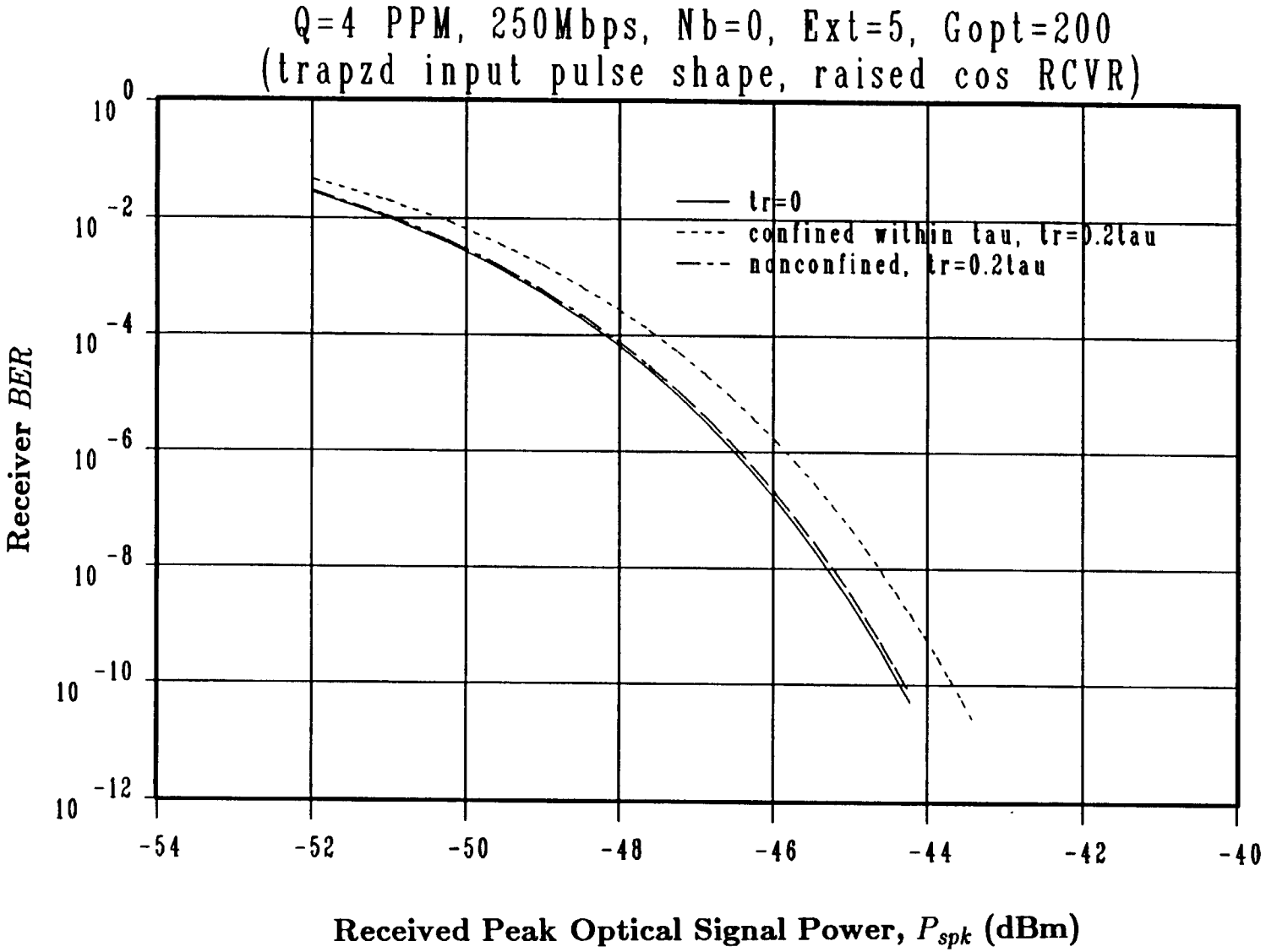

Figure 11. Raised cosine filter receiver performance for rectangular and trapezoidal input pulse shapes which are confined and not confined within a PPM time slot.

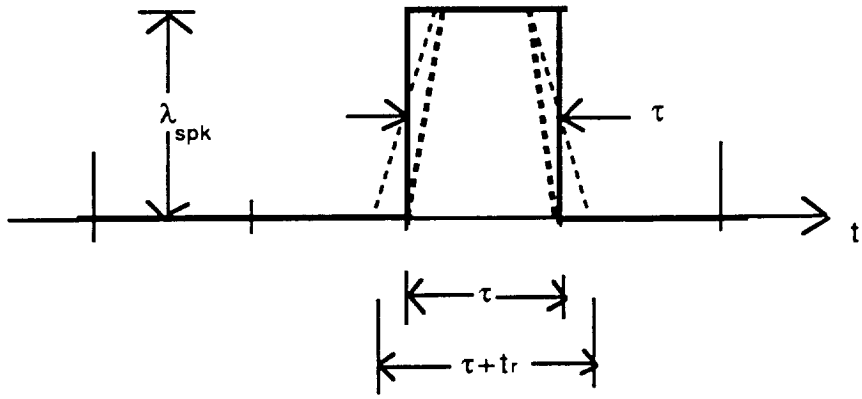

Figure 12. Confined (heavy dashed line) and nonconfined (light dashed line) trapezoidal input pulse shapes used for computing the curves in Figure 11.

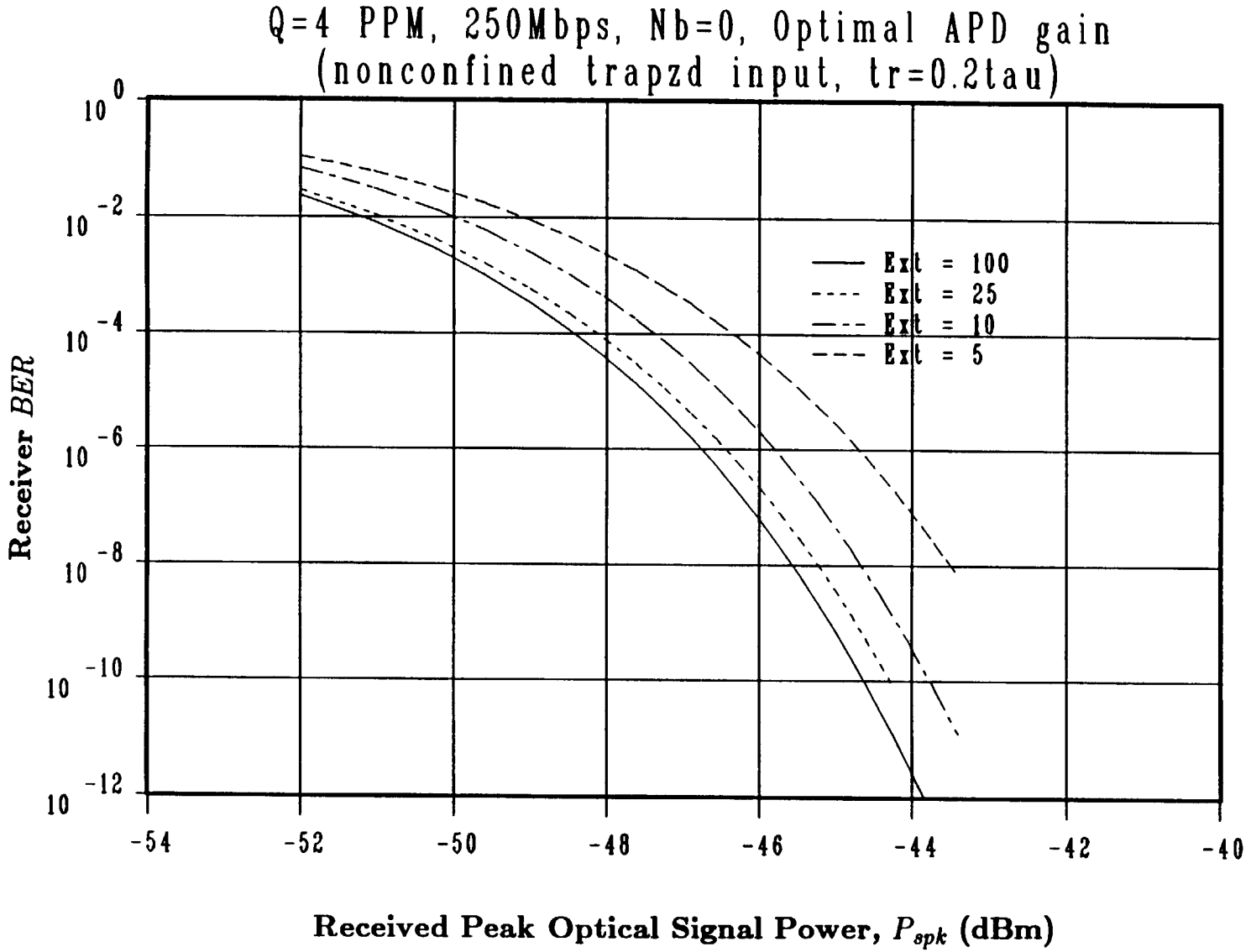

Figure 13. Raised cosine filter receiver performance under different laser ON-OFF extinction ratios.

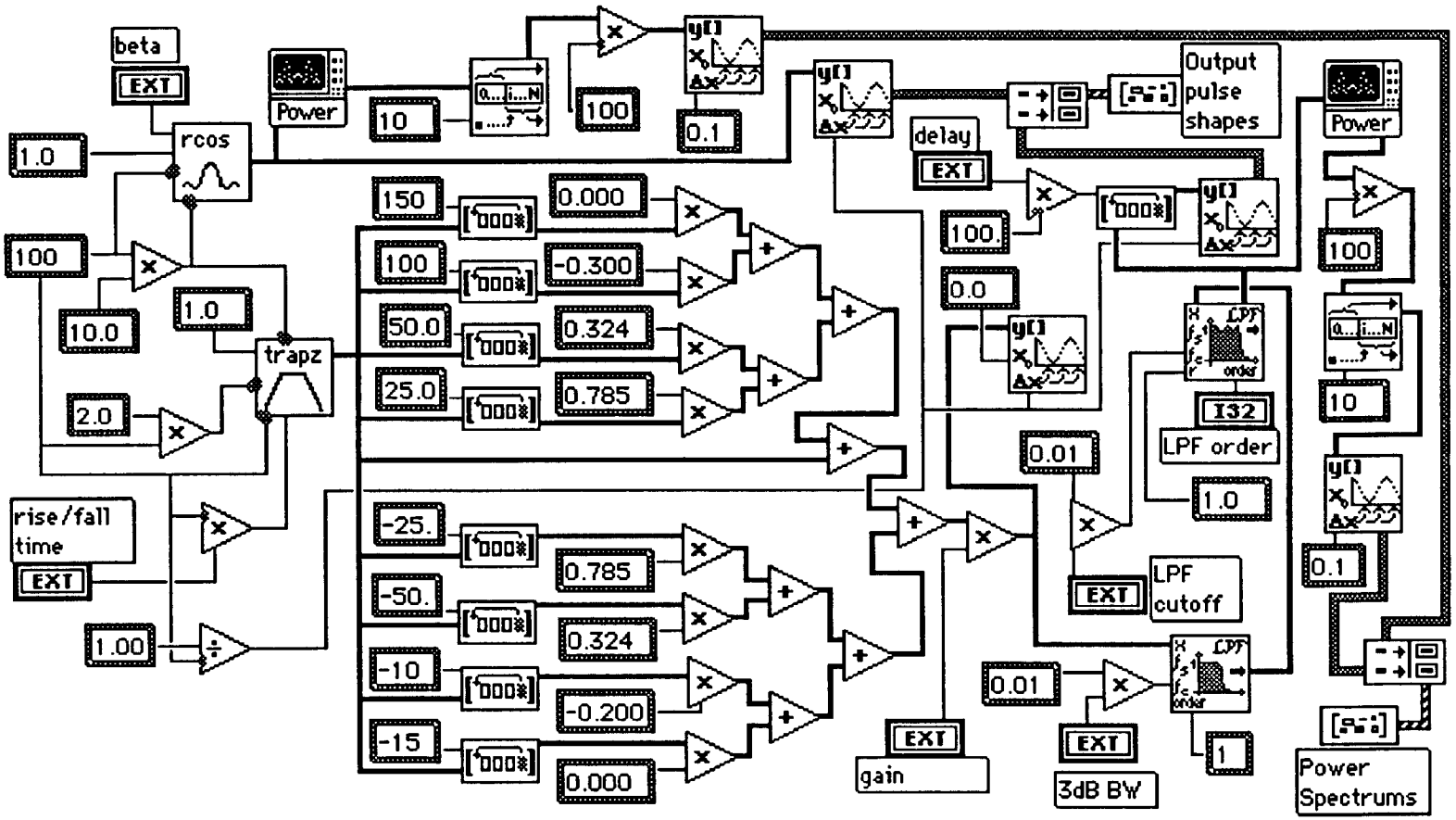

Figure 14. The LabView program used in the computer simulation of the transversal raised cosine filter.

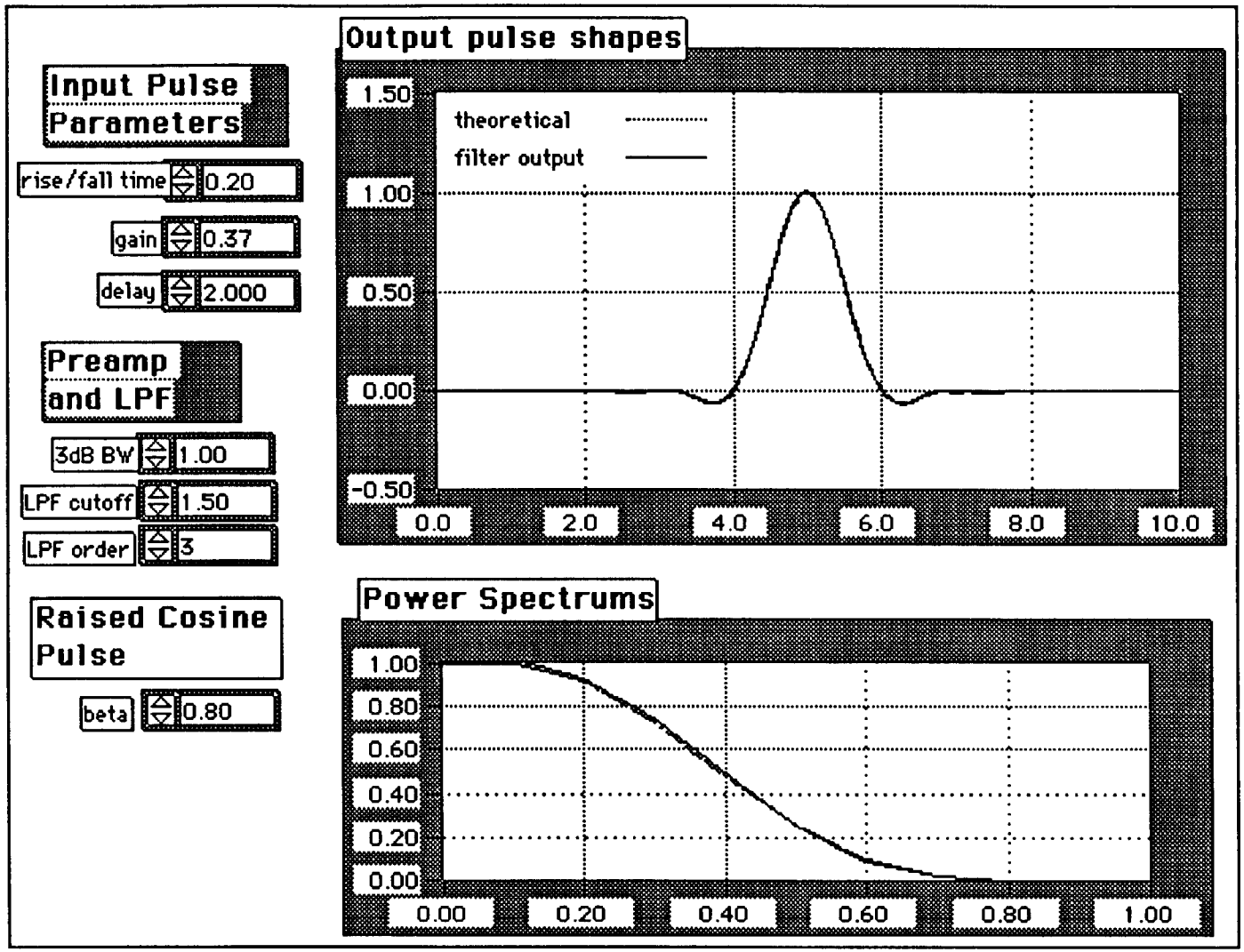

Figure 15. Computer simulation result of the transversal raised cosine filter.

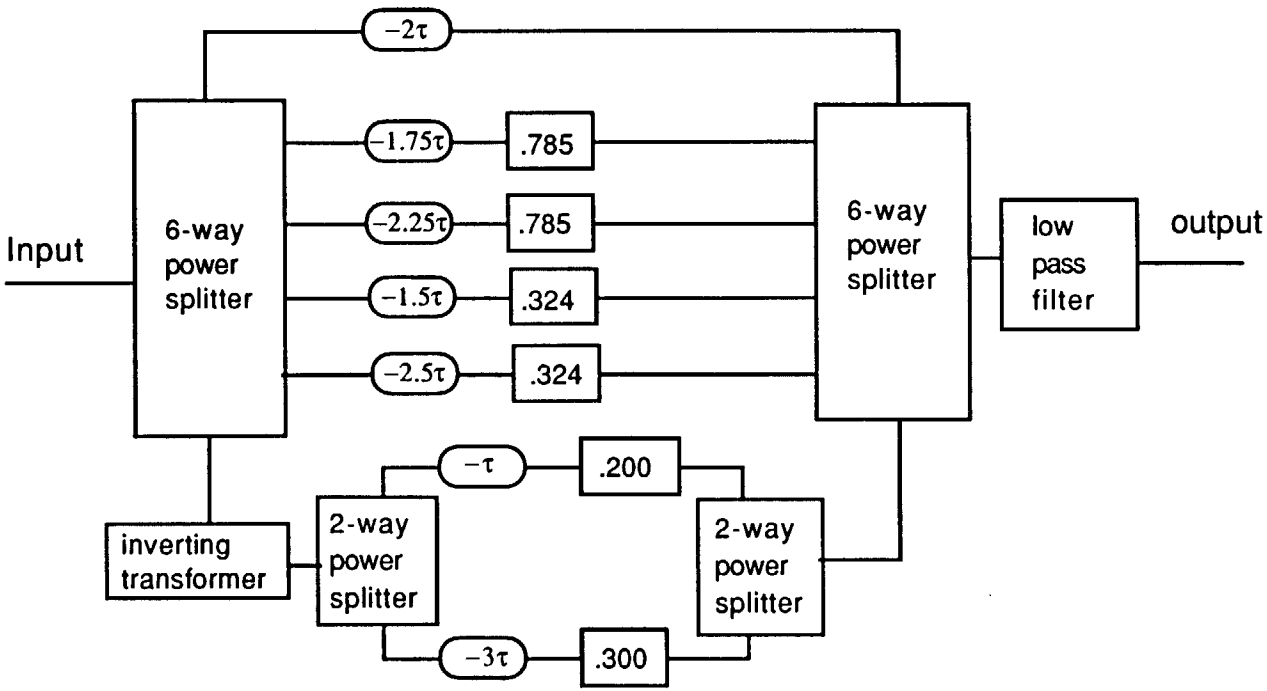

Figure 16. Circuit diagram of a transversal raised cosine filter for a 4-ary PPM receiver.

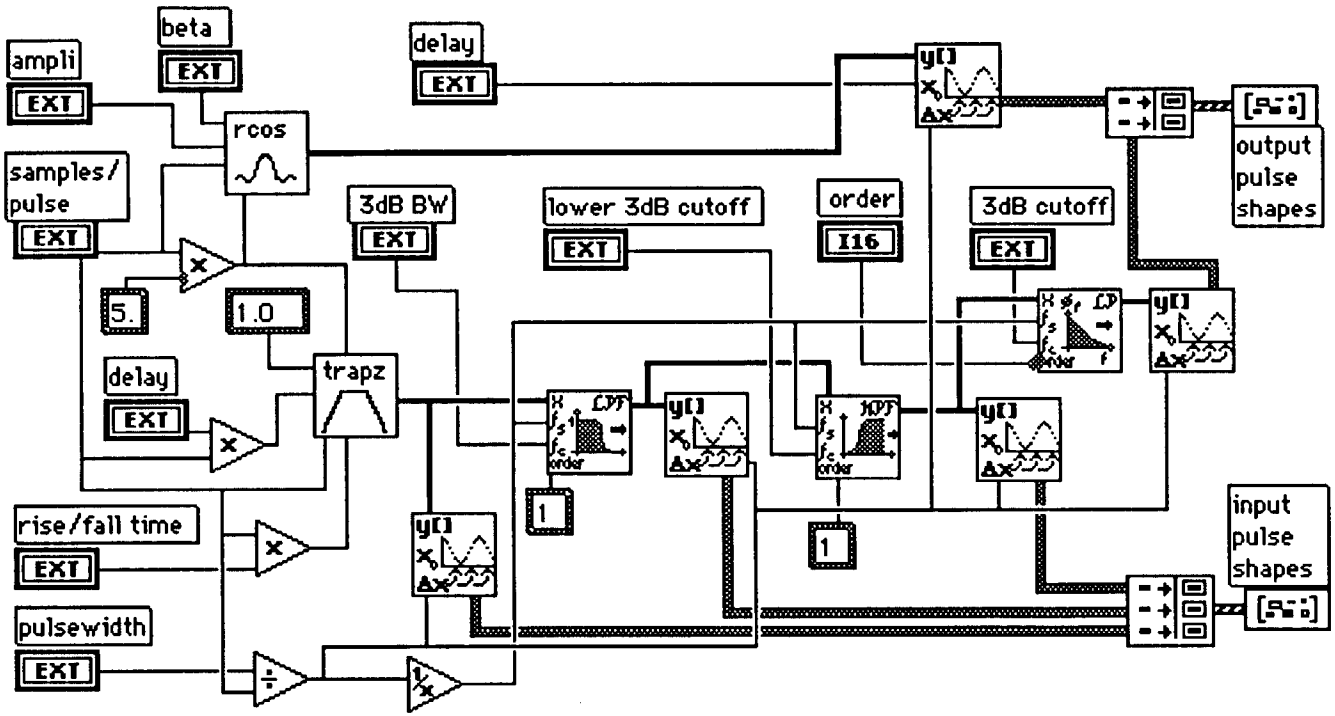

Figure 17. The LabView program used in the computer simulation of the Bessel lowpass filter as an approximate raised cosine filter.

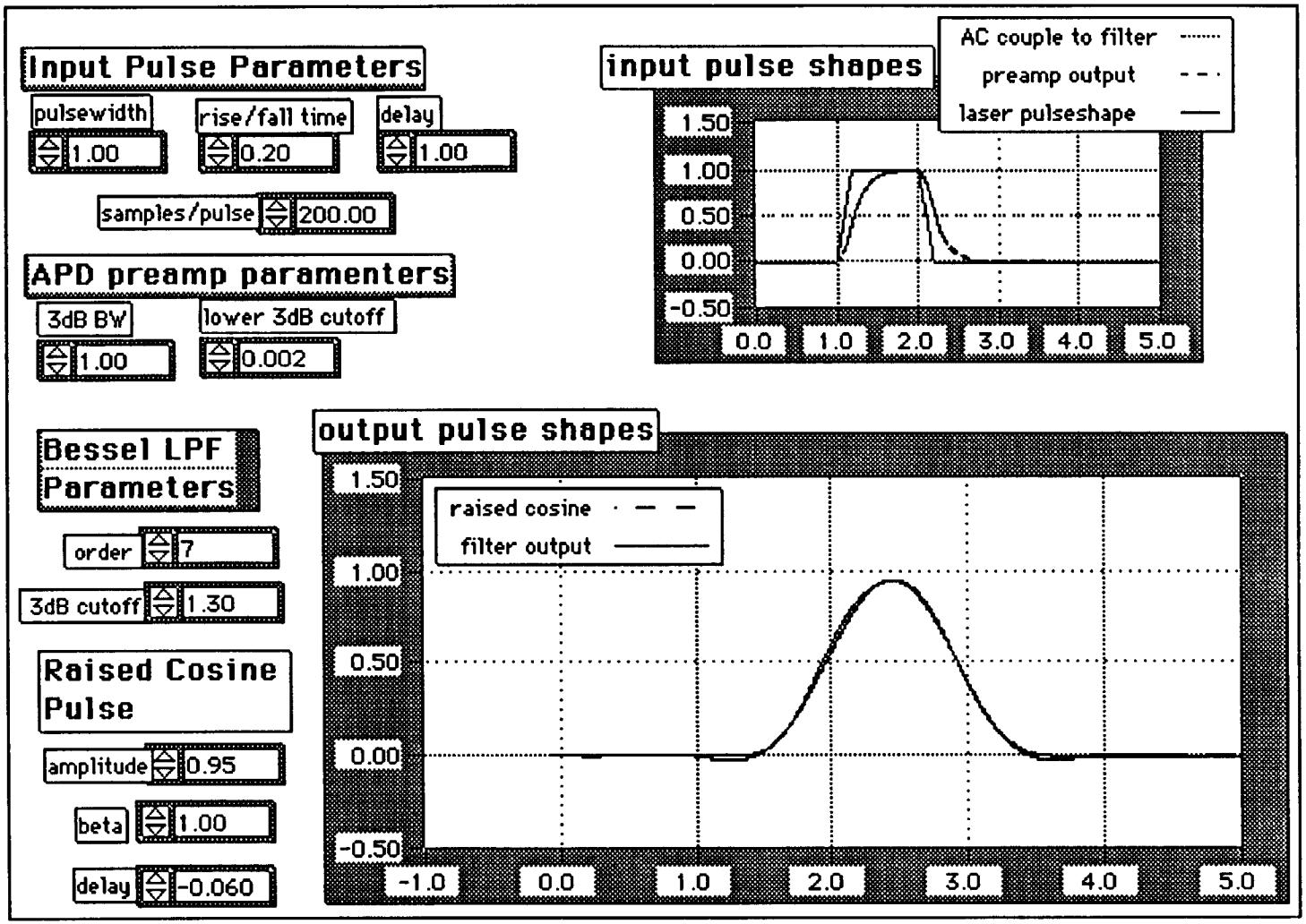

Figure 18. Computer simulation result of the Bessel lowpass filter as a raised cosine filter.

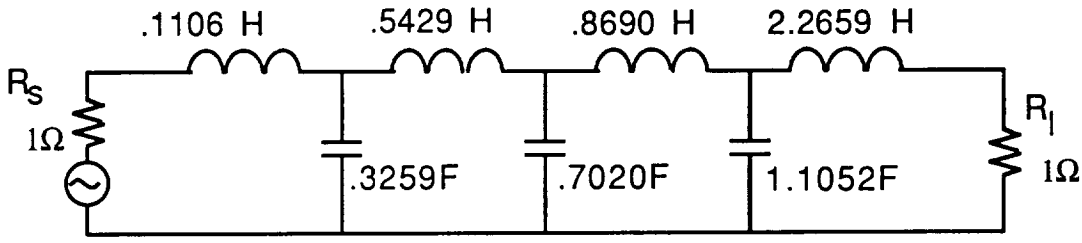

(a). Normalized 7th order Besses lowpass filter
($2\pi f_{3dB}$= 1 rad/sec., Rs=Rl=1Ω).

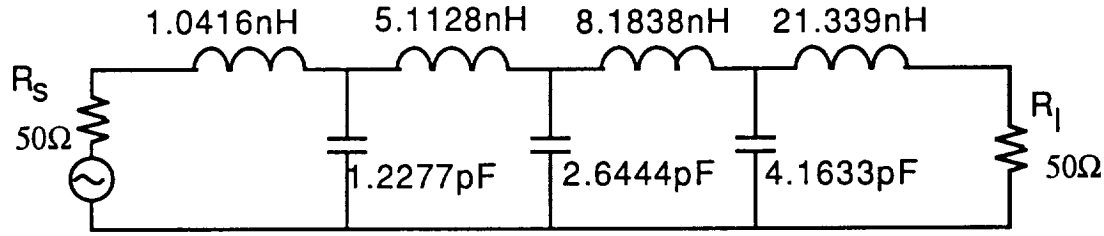

(b). Unnormalized 7th order Besses lowpass filter
(f_{3dB}=845MHz, Rs=Rl=50Ω)

Scalling: $C=C_n /2\pi f_{3dB}R$, and $L=L_n R/2\pi f_{3dB}$

Figure 19. Example circuit diagram of a 7th order Bessel lowpass filter with a 3 dB bandwidth equal to 845 MHz.

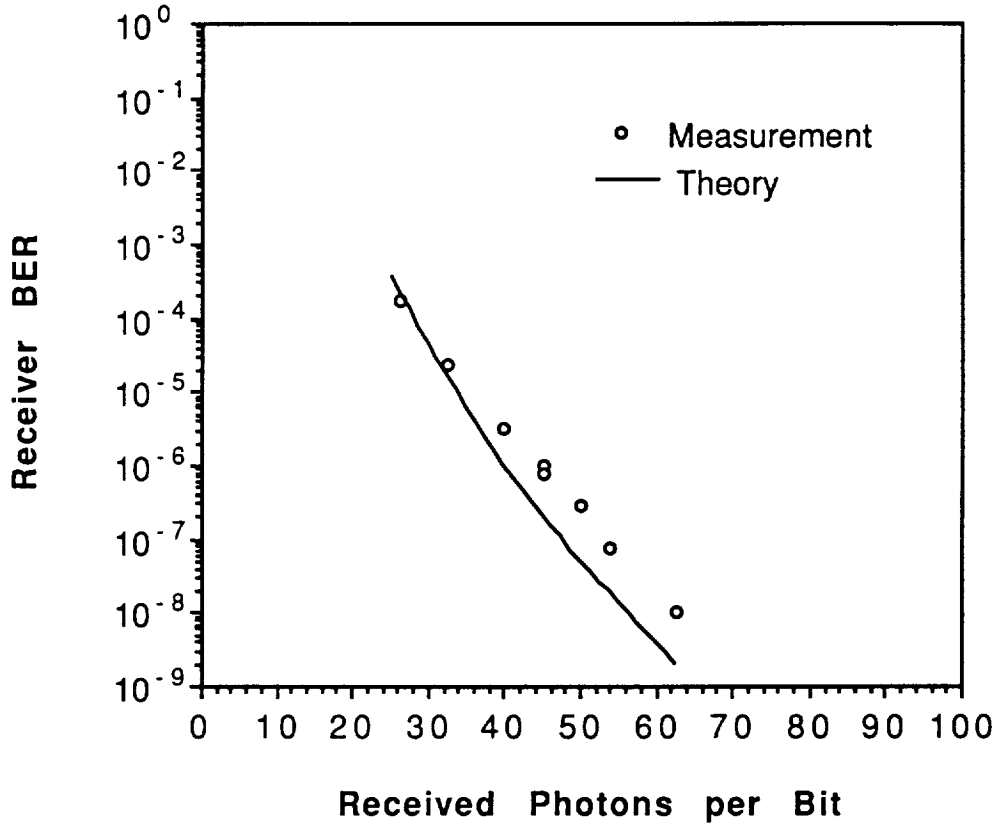

Figure 20. Receiver performance of the 50 Mbps 4-ary PPM receiver with a ML filter and the PlessCor APD preamplifier module. The circles represent the measurement data and the solid curve represents the theoretical calculation.

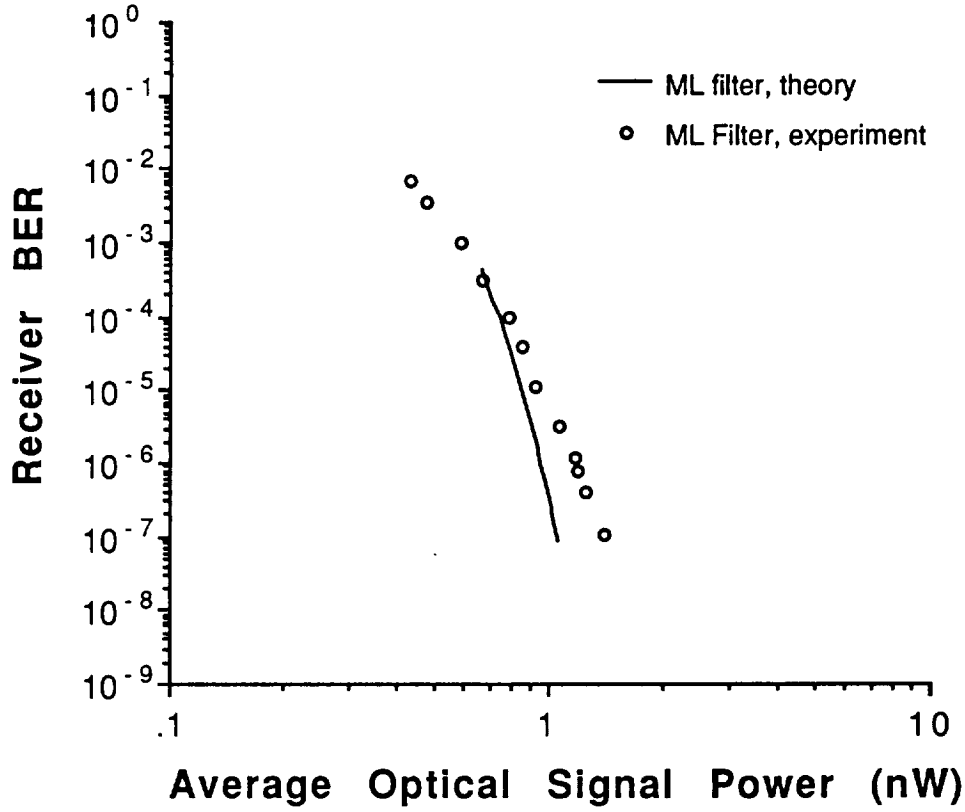

Figure 21. Receiver performance of the 50 Mbps 4-ary PPM receiver with ML filter and the EG&G Slik APD preamplifier module. The circles represent the measurement data and the solid curve represents the theoretical calculation.

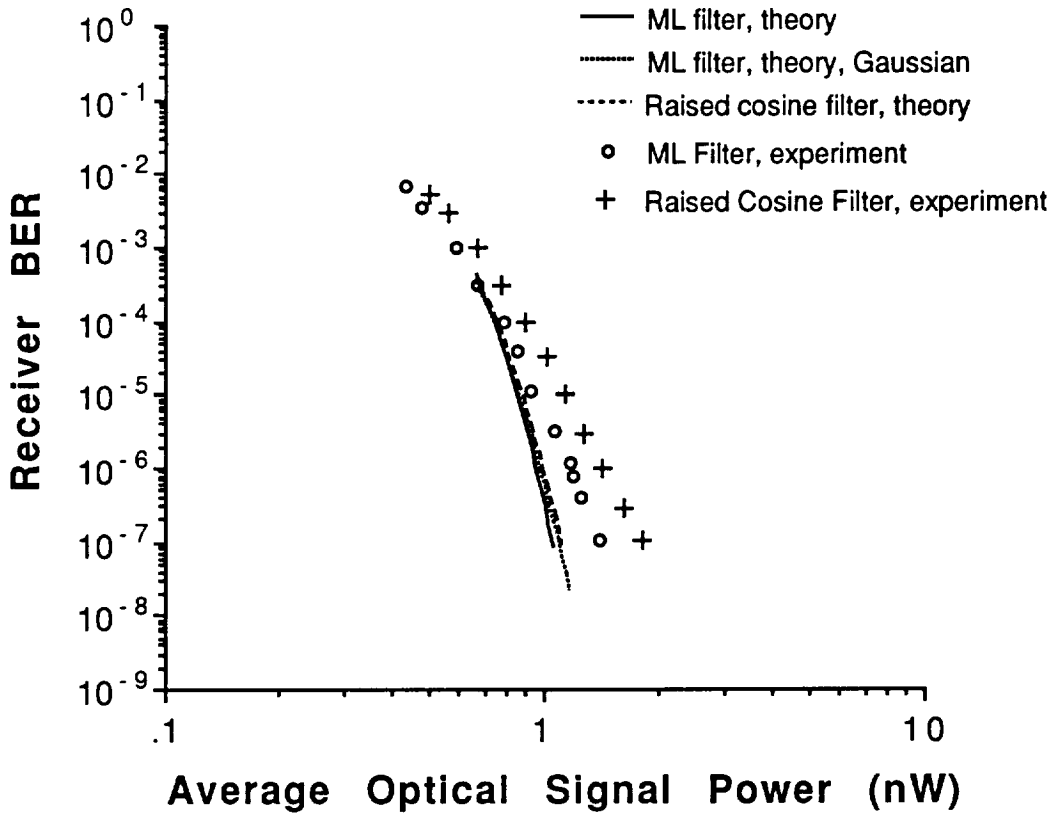

Figure 22. Receiver performance of the 50 Mbps 4-ary PPM receiver with ML filter (circles) and Bessel lowpass filter (crosses) and the EG&G Slik APD preamplifier module. The solid curve represents the theoretical calculation using the nearly exact analyses, the dotted curve represents the calculation for ML filter receiver using Gaussian approximation, and the dashed curve represents the calculation for raised cosine filter receiver using Gaussian approximation. The APD gain was G=140 for both measurement data and theoretical analysis.

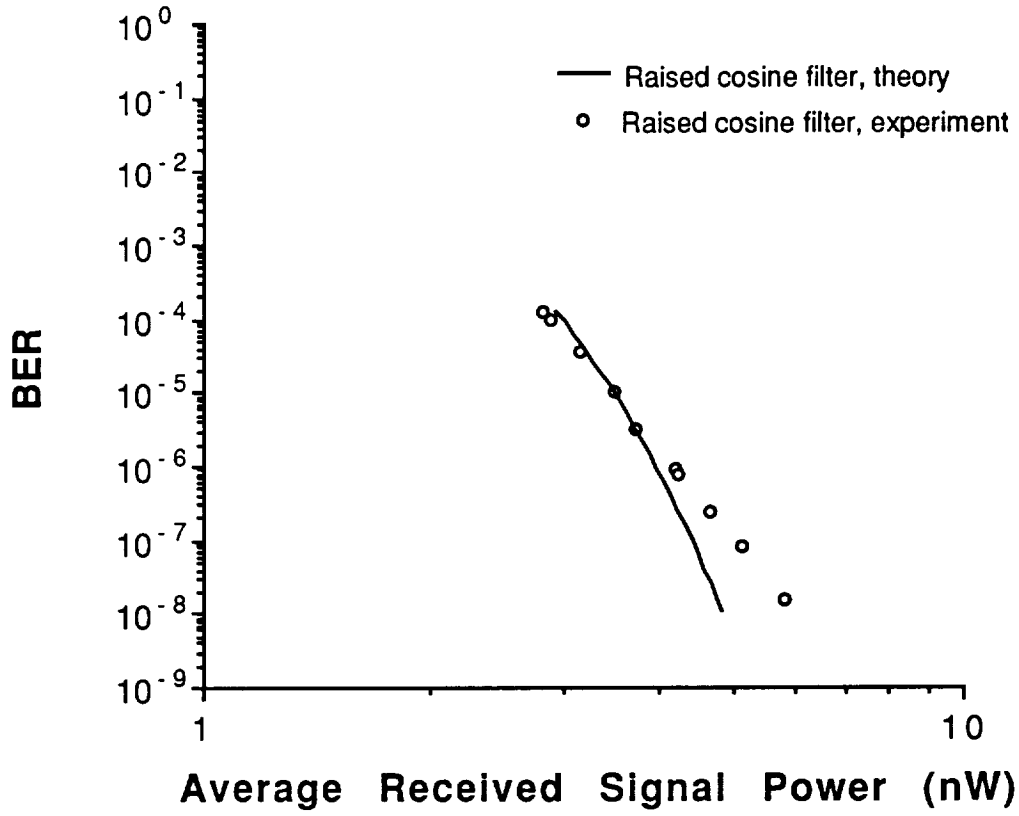

Figure 23. Receiver performance of the 220 Mbps 4-ary PPM receiver with a Bessel lowpass filter and the EG&G Slik APD preamplifier module. The circles represent the measurement data and the solid curve represents the theoretical calculation using Gaussian approximation. The average APD gain was G=69 for both experiment and theoretical calculation.